A fully-actuated quadcopter representation using quaternions

J. Cariño, Hernan Abaunza, Pedro Castillo Garcia

A Fully-Actuated Quadcopter Representation using Quaternions

J. Cariño[a,*], H. Abaunza[b], P. Castillo[a]

[a] Université de technologie de Compiègne, CNRS, Heudiasyc (Heuristics and Diagnosis of Complex Systems), CS 60319 - 60203 Compiégne Cedex, France; [b] Tecnológico de Monterrey, Escuela de Ingeniería y Ciencias, Av. General Ramón Corona 2514, 45201 Zapopan, Jalisco, México.

ARTICLE HISTORY
Compiled September 10, 2022

ABSTRACT
Recent advances in practical fields like robotics and the miniaturization of many sensors and actuators have turned autonomous vehicles into a reality. These systems come in many shapes and forms depending on the medium and their design, but can be classified in one of two categories according to their mechanical configuration and number of actuators: fully actuated and under actuated vehicles, the second group still poses many challenges for the automatic control and robotics communities. This work introduces an easy methodology, based on quaternions, for designing controllers for a class of under-actuated systems, such as multicopter vehicles. The methodology starts from a fully actuated representation of the system and adapts it to be implemented in under actuated systems. In addition, it allows the easy development of controllers without take on care the coupled dynamics of the system. The proposed approach is based on Lyapunov's stability theory and is proven for certain criteria of the system's dynamics. The quadcopter configuration is used to validate the proposed methodology in simulations and in experimental tests.

KEYWORDS
Quaternion, quadcopter, UAV, multirotor, nonlinear dynamics, under-actuated system, model representation

Abbreviations:

DoF	Degree(s) of Freedom
UAV	Unmanned Aerial Vehicle
AGV	Autonomous Ground Vehicle
AUV	Autonomous Underwater Vehicle
SFC	State Feedback Controller
ESC	Energy Shaping Controller
SSC	Separated Saturations Controller

[*]Corresponding author. Email: jossue.escobar@hds.utc.fr. ORCID: https://orcid.org/0000-0002-1747-7740
H. Abaunza Email: habaunza@tec.mx
P. Castillo Email: castillo@hds.utc.fr

1. Introduction

Autonomous vehicles, also known as unmanned systems in a more general view, are the inevitable result of modern industrialization and electronic miniaturization. Recent advances have shortened the time between the development of these autonomous systems and their application to the point that autonomous vehicles are already being actively used to some degree in multiple fields. New evidence seems to imply that there are many advantages towards a more widespread adoption of these kinds of systems, including, but not limited to, the reduction of greenhouse emissions between 5% and 60% and up to 90% less fuel consumption in the whole transportation industry as a whole according to Kopelias, Demiridi, Vogiatzis, Skabardonis, and Zafiropoulou (2020). The emergence of an integrated transportation infrastructure which is already underway, including policy making, and it is starting with autonomous vehicles according to Li, Sui, Xiao, and Chahine (2019) and Hancock, Nourbakhsh, and Stewart (2019). One of the main subjects in the technical end of unmanned systems is the ability for these to withstand uncertainties, which helps to ensure a safe environment for the people that use and interact with them. In essence, autonomous vehicle's safety can be directly tied with the robustness property from a control perspective.

Unmanned systems come in a wide variety of forms and shapes, but they are often modeled as rigid bodies moving in a 3D environment. For example, Autonomous Ground Vehicles (AGVs) tend to be limited to a planar movement while Unmanned Aerial Vehicles (UAVs) and Autonomous Underwater Vehicle (AUVs) have a disposition to move anywhere in a 3D environment. In this regard, autonomous vehicles can be classified as either fully actuated or under actuated, depending on the amount and configuration of their actuators and their degrees of freedom (DoF). Fully actuated rigid bodies can move in all six DoF of a 3D environment. Three coordinates are used to establish their position in a 3D space while at minimum three coordinates are required to provide enough information to obtain its orientation. Under actuated systems have fewer than six DoF *i.e.* their movement is either restricted to a plane or other spatial construct with fewer than six DoF, or one or more of their DoF are dependent among each other. In the later case, the system is said to have coupled dynamics. This work focuses mainly on one family of vehicles amid all the under actuated rigid bodies with coupled dynamics systems. The main characteristic of this group is that the thrust force, which is generated by the actuators and is considered a control input, has a fixed direction in the body frame *i.e.* the only feasible way to change the vehicle's position is by also changing its attitude, effectively coupling the translation system with the orientation one. There are many types of vehicles that belong to this family of systems, including multicopters, certain classes of underwater vehicles and even autonomous ground vehicles can be modeled as a special case of this family of systems.

In general, the design of a control strategy for a fully actuated autonomous platform is straightforward because a control law can be designed and proven stable independently for each DoF. In sharp contrast, the control design of under actuated systems with coupled dynamics represents a more complex challenge, which is the main reason why it is still an active research subject. A common solution for this problem is to use an internal attitude control loop to guide the actuator's force with an outer control loop. Some examples of this approach include the works presented in Kumar et al. (2020), Colmenares-Vázquez, Marchand, Castillo, and Gómez-Balderas (2017), Shastry, Bhargavapuri, Kothari, and Sahoo (2018), Islam, Okasha, Idres, and Mansor (2018), Islam and Okasha (2019) and Lees-Miller, Hammersley, and Wilson (2010), to name a few recent works. This is commonly referred in the literature as the principle of separation or high and low control levels. The main disadvantage of this design method is that even when the stability of each individual control can be proven, the stability of the coupled control is not a trivial matter. Control laws implemented using this design principle require that the position control have a much smaller effect on the global control strategy than the attitude controller in order to guarantee practical stability. The proposed control design methodology takes into account the coupling of the high and low control levels in order to guarantee almost global stability using the Lyapunov formalism. The only restrictions come from the physical constraints imposed by the characteristics of the proposed family of systems.

Many of the models presented in contemporary works such as Antonio-Toledo, Sanchez, Alanis, Flórez, and Perez-Cisneros (2018), Pratama, Muis, Subiantoro, Djemai, and Ben Atitallah (2018), Labbadi and Cherkaoui (2019), and Ahmad, Kumar, Bhandari, and Patil (2020), still use Euler angles for the description of the attitude dynamics. This is one of the most widely used forms to represent the orientation of an aerial vehicle and its main advantage is that they can be considered as an intuitive way to describe the attitude of an aerial vehicle. However, the intention of any control law applied to an autonomous vehicle is to have a computer, or a similar machine, replace the tasks of the pilot. In this sense, the attitude representation of the mathematical model is not trivial, as some representations tend to be more suited for implementation as a control law. In this regard, Euler angles present some serious disadvantages for the design and implementation of controllers, like the overhead trigonometric calculations needed in order to rotate a vector from one reference frame into another. Other attitude representations can be found in Shuster (1993), of which the main ones used in the context of autonomous vehicles include rotation matrices and unit quaternions. In contrast with Euler angles, unit quaternions are numerically more stable, because one can normalize them in order to mitigate the effect of angle drift, and avoid the gimbal lock problem as stated in Morais, Georgiev, and Sprößig (2014b), which often causes discontinuities in the implementation of control laws. Rotation matrices are another formalism that is resilient to angle drift and avoids singularities. However, unit quaternions use less space, as they store four numbers instead of the nine required by rotation matrices, and require less operations in order to rotate a single vector from one reference frame into another. There is also the requirement that rotation matrices need to be orthonormalized in order to be resilient to numerical rounding errors, which is less efficient than just normalizing a quaternion. The most common detriment for using unit quaternions in this context is due to the unwielding effect. This issue allows exactly two unit quaternions to describe the same attitude state at any one time, but can be eliminated if a restriction is applied to the range of the scalar part. Because of the properties that unit quaternions have in the description and implementation of attitude controllers, research into autonomous vehicles is turning away from Euler angles and adopting unit quaternions as the standard, which can be seen in works such as Ariyibi and Tekinalp (2020) and Lu, Ren, and Parameswaran (2020).

A key aspect of this work is the use of quaternions for the modeling and description of the attitude dynamics in the proposed control law design. Using a strategy similar to the principle of separation, a desired attitude quaternion is calculated and given to the orientation controller that allows the body-fixed thrust of the vehicle to match the desired force of the position controller. One of the cornerstone works in the determination of this desired quaternion is from Markley (2002), which is used in most of the control strategies that deal with attitude tracking using quaternions. An alternative proof for the desired quaternion formula is derived and presented in this work using geometric properties and quaternion algebra, including the quaternion exponential and logarithm functions as described in Morais, Georgiev, and Sprößig (2014a). Displaying the formula in this manner facilitates the determination of the effects of the attitude dynamics for the global stability proof.

The main contribution of our work is to present a control design methodology for a particular family of under actuated systems. The proposed technique uses the concept of an equivalent virtual system that has the same physical properties as the real system, like mass and shape, but is considered to be fully actuated. Our approach starts with a control scheme designed for this equivalent system, which will become the template of a proposed control law. The idea is to facilitate the design the controller for the under actuated system from this virtual control scheme such that the controlled under actuated system has similar dynamics to the controlled virtual fully actuated system. Stability of these new control inputs is proven using the Lyapunov formalism. Unmodeled dynamics can be analyzed as perturbations and a condition for the stability of the under actuated system is presented based on the virtual controller for the fully actuated system.

The key advantage of our technique is the generic implementation approach. Similar to how Lyapunov analysis is used to verify stability in dynamic systems, the proposed method

establishes conditions and properties that a virtual fully actuated control law needs to have in order to be implemented in the proposed under actuated systems. This can be used to complement or even expand on the control design for this particular family of systems.

Three example cases of the proposed process are introduced for illustrating the advantages that our method offers with respect to other approaches. The first one uses a feedback control for the equivalent fully actuated system and it is demonstrated that a linear control law can be adapted for this kind of under actuated systems without linearize the system. R1Q1

The second example is a passivity-based control that stabilizes the vehicle by changing the potential energy of the overall system and injecting a dampening effect as seen in Brogliato, Maschke, Lozano, and Egeland (2007). This energy shaping controller displays the capacity of the method to adapt even to control strategies that involve physical properties of the platform, like its kinetic energy dissipation and potential energy shape. The last proposed control law is a non-linear strategy known as a separated saturations controller, which is used for stabilizing a class of linear systems. Saturated controls have been proposed and studied in works like Castillo, Dzul, and Lozano (2004), Xie and Lynch (2017) and Alatorre, Castillo, and Mondié (2016) and applied in nonlinear systems. The main difference between these methods and the proposed example is that it is shown in the Lyapunov analysis that the use of a saturated position control makes the quadcopter system more robust, it is mainly due the fact that, in our approach we consider the nonlinear system and not only its linear part.

The outline of the paper is presented as follows. In Section 2, preliminary concepts such as the dynamic model of a rigid body are introduced. Here, we also include our case study. In Section 3 the proposed control design methodology is presented in detail and its stability proof based on the Lyapunov analysis is also included. In Section 4 the proposed methodology is applied in a quadcopter platform by adapting three different control strategies from a fully actuated equivalent model is described. The control algorithms were numerically simulated and also experimentally tested using a physical quadcopter vehicle. The results of these tests are presented in Section 5. Finally, the conclusions of the work are shown in Section 6. Appendix A is included for providing a brief background in quaternion arithmetic and kinematics.

2. Preliminaries and problem statement

Remark 1. Quaternion variables are shown in **bold**, like $\boldsymbol{q} \in \mathbb{H}$. Vectors are presented with arrows as $\vec{\Omega} \in \mathbb{R}^3$, and each of its elements using sub-indexes as $\vec{\Omega} \coloneqq [\Omega_x \ \ \Omega_y \ \ \Omega_z]^T$. Scalars are simply written as lowercase letters $a \in \mathbb{R}$, and vector norms are described as $\|\vec{v}\| \in \mathbb{R}_+$.

Normalized vectors are described as $\hat{v} \coloneqq \dfrac{\vec{v}}{\|\vec{v}\|} \in \mathbb{R}^3$, while matrices are written as uppercase letters $A \in \mathbb{R}^{n \times m}$.

The identity matrix is written as I_n, where $n \in \mathbb{Z}$ is the dimension of the matrix.

The family of vehicles addressed in this work consists of any system that can be modeled as a six degrees of freedom rigid body, where its attitude is completely actuated and its position depends on a body-fixed thrust force affected by the gravity on the system (or any other constant force). The main examples for this kind of vehicles are multi-copter aircrafts and some kinds of under-water vehicles. The quadcopter vehicle will be used as a case of study for developing the approach.

Rotors, in multi-copter vehicles, are usually designed without switch-plates. The rotor's force acts in a fixed direction, which is parallel to an axis in the body frame (usually the z axis). This, combined with the fact that these aerial robots are commonly under-actuated, implies that the translation dynamics are coupled with its attitude dynamics. This characteristic still represents a challenge for the automatic control community.

Consider the following Newton-Euler model defining the mathematical representation of a rigid body perturbed by external disturbances, in our case the rigid body is the quadcopter

aerial vehicle

$$m\ddot{\vec{p}} = R\begin{bmatrix} 0 \\ 0 \\ \sum_i f_i \end{bmatrix} + m\vec{g} + \vec{\zeta}_p. \quad (1)$$

$$J\dot{\vec{\Omega}} = \vec{\tau} - \vec{\Omega} \times J\vec{\Omega} + \vec{\zeta}_\Omega \quad (2)$$

where m and J are the system's mass and inertia tensor, respectively. $\vec{\Omega}$ represents the angular velocity w.r.t. the body frame. $\vec{p}$ denotes the position vector of the system w.r.t. the inertial reference frame. The term $\sum_i f_i$ describes the effects of the forces produced by motors on the rigid body. $\vec{\tau}$ denotes the motor's torques while $R \in SO(3)$ symbolizes a rotation matrix. The effect of the gravity on the system is denoted by $\vec{g} \in \mathbb{R}^3$. The vector $\vec{\zeta}_k \in \mathbb{R}^3; \forall k \in \left\{\vec{p}, \vec{\Omega}\right\}$ represents nonlinear uncertainties like drag effects and/or wind turbulence.

The forces, f_i and the torques, τ_i, in multi-rotor systems are usually related with the angular velocity of the rotors (ω_i), their forms depend in general of the number of actuators (rotors) and the configuration of its arrangements. In addition, in these rotor craft vehicles its rotational dynamics contains three torques and is considered actuated. The quadcopter vehicle represents the most popular multi-rotor configuration, see Figure 1.

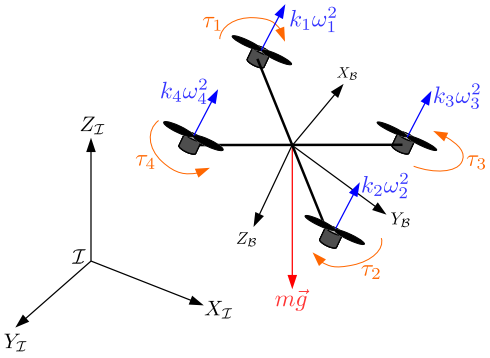

Figure 1.: Quadcopter configuration. Each rotor produces a force $f_i \sim k_i\omega_i^2$; where k_i is a constant aerodynamic parameter and ω_i denotes the angular rate of motor i. τ_i introduces the torque produced by motor i. $\mathcal{I} = X_I, Y_I, Z_I$ signifies the inertial frame and X_B, Y_B, Z_B means the body frame.

The rotation matrix R, in (1), is one of the most commonly used methods to represent the translational forces acting in the body frame to the inertial frame, or vice versa. In this work a unit quaternion is used to represent the attitude of the system. Its relation with the forces acting on the rigid body is explained in the following remark.

Remark 2. A rotation operation can be seen as a rigid transformation on a real three dimensional space with the following properties:

- The position of the origin does not change.
- It is linear.
- It can be represented by an orthonormal rotation matrix.
- It does not affect the magnitude.

Further properties and discussions can be seen on Kalman (1989) and (Goldstein, Poole, & Safko, 2002, Chapter 4). The rotation operation applied to any three-dimensional vector $\vec{v} \in \mathbb{R}^3$ with these properties will be described as $R_q(\boldsymbol{q}, \vec{v})$, which can be accomplished with a triple quaternion product as

R1Q3

$$\vec{v}' = R_q(\boldsymbol{q}, \vec{v}) = \boldsymbol{q}^* \otimes \vec{v} \otimes \boldsymbol{q}. \quad (3)$$

where

$$\boldsymbol{q} \coloneqq cos\left(\frac{\varpi}{2}\right) + \hat{n}\, sin\left(\frac{\varpi}{2}\right) \tag{4}$$

where $\hat{n} \in \mathbb{R}^3$ is a unit vector representing the vehicle's rotation axis and $\varpi \in \mathbb{R}$ its rotation angle. Vectors $\vec{v} \in \mathbb{R}^3$ are considered as pure quaternions with zero scalar part. $\vec{v}'$ is referenced in the body frame while $\vec{v}$ is located in the inertial frame. The operator $R_q(\boldsymbol{q}, v)$ is linear as proved in Morais et al. (2014b).

System (1)- (2) for multi-rotors with parallel motors can be also written using the quaternion representation as

$$m\,\ddot{\vec{p}} = \boldsymbol{q} \otimes \vec{F}_{th} \otimes \boldsymbol{q}^* + m\vec{g} + \vec{\zeta}_p \tag{5}$$

$$J\,\dot{\vec{\Omega}} = \vec{\tau} - \vec{\Omega} \times J\,\vec{\Omega} + \vec{\zeta}_\Omega \tag{6}$$

where

$$\vec{F}_{th} \coloneqq \begin{bmatrix} 0 \\ 0 \\ \sum\limits_i f_i \end{bmatrix} \tag{7}$$

is the vehicle's thrust force vector in the body frame; its magnitude is often considered as a control input, however, note its effect in the inertial frame directly depends on the system's attitude. The term $\boldsymbol{q} \in \mathbb{H}$ is the system's orientation in unit quaternion form and $\boldsymbol{q}^*$ denotes its conjugate term[1].

From (5)- (6) notice that the actuation force is expressed in the inertial frame and can be obtained from the thrust force $\vec{F}_{th}$ using the quaternion rotation operation. Observe also that systems (1)- (2) and (5)- (6) are equivalent and both are under-actuated.

From literature, it can be appreciated that several control algorithms have been proposed for controlling an aerial system represented in (1)- (2). Most of them use the principle of separation for stabilizing the translational and the rotational dynamics (also known as high and low control level in aerial vehicles community), others ones use the complete system for designing the control algorithm in which some control inputs are used to stabilize more than one DoF. The results are interesting and the control performance is well demonstrated in most cases. When using the principle of separation the direction of the main thrust is usually given by the roll and pitch dynamics. These angular dynamics governs the translational position in the horizontal plane x, y, thus, it is easy to represent the longitudinal and lateral dynamics of the aerial vehicle with respect to desired roll ($\phi_d \sim f(y, \dot{y})$) and pitch ($\theta_d \sim f(x, \dot{x})$) angles. The problem arising here is the multitude of solutions for representing these angles and sometimes produce undesirable performances in the aerial vehicle. In addition, the altitude performance is degraded with an undesired damping when moving in lateral or longitudinal axis.

Nevertheless, the high non linearity of this representation, due to coupled dynamics, is troublesome and tedious to deal with when designing global control strategies for the full system. This is the main reason why this principle is proven stable either locally or just for some parts of the system or particular cases. Some examples can be seen using energy-based or passivity methodologies El-Badawy and Bakr (2016) -Kottenstette and Porter (2009).

[1] details of $\boldsymbol{q}^*$ see (A.2)

3. Virtual fully actuated dynamic model

In our approach, we propose a virtual fully actuated dynamic model for (5) – (6) based on a unique desired quaternion avoiding multiple solutions to orientate the main thrust of the vehicle. This solution offers a natural principle of separation between both dynamics (translational and rotational) and allows the design to easily separate the control algorithms considering each subsystem a different system from one another. In addition, our approach differs from those previously explained in that it produces the exact combination of the quadcopter's attitude and thrust force necessary to change the translational dynamics in order to have a desired position control. This result is exact and prevents the need of making further hypothesis on the system due to approximations.

Therefore, the goal will be to to define the desired quaternion, $\boldsymbol{q}_d \in \mathbb{H}$, fulfilling these properties, such that, for given controllers $\vec{F}_{th}$ and $\vec{\tau}$ stabilizing the whole system,

$$\left.\begin{array}{l} \vec{p} \to \vec{p}_d \\ \boldsymbol{q} \to \boldsymbol{q}_d \end{array}\right\} \implies t \to \infty \tag{8}$$

where $\vec{p}_d(\cdot) \in \mathbb{R}^3$ defines a desired vector position and t is the time.

3.1. Desired quaternion characterization

Some necessary mathematical definitions are introduced to compute the desired quaternion.

Definition 1. Since the rotation operator does not affect the norm of a vector, the group where this operator works can be limited to the set

$$\Lambda = \left\{ \vec{v} \in \mathbb{R}^3 : \|\vec{v}\| = 1 \right\}. \tag{9}$$

Any vector in $\mathbb{R}^3$ can be mapped to a corresponding vector in Λ by normalizing it.

Definition 2. An orthogonal unit vector group χ given two non-zero arbitrary normalized vectors $\hat{a}, \hat{b} \in \Lambda$ can be defined as

$$\chi\left(\hat{a}, \hat{b}\right) = \left\{ \hat{v} \in \Lambda : \left(\hat{a} - \hat{b}\right) \cdot \hat{v} = 0 \right\} \tag{10}$$

From Definition 2, observe that the set χ incorporates all unit vectors that are perpendicular to the difference between $\hat{a}$ and $\hat{b}$ and is the set that contains all possible values of $\hat{n}$ for the given vectors. This is explained in the following Lemma 1.

Lemma 1. Given non-zero unitary vectors $\hat{a}, \hat{b}, \hat{n} \in \Lambda$, the rotation operation $R_q(\cdot)$, transforms vector $\hat{a}$ into vector $\hat{b}$, by rotating around axis $\hat{n} \iff \hat{n} \in \chi$ with a rotation angle $\varpi(\hat{a}, \hat{b}, \hat{n})$.

Proof. The sufficiency can be seen from the definition of rotation. The rotation operation does not affect the component of $\hat{a}$ parallel to the rotation axis $\hat{n}$ nor its counterpart for $\hat{b}$, which can be calculated as

$$\begin{array}{rcl} \hat{a}_{\parallel} & \coloneqq & \hat{a} \cdot \hat{n} \\ \hat{b}_{\parallel} & \coloneqq & \hat{b} \cdot \hat{n} \end{array} \tag{11}$$

This implies that $\hat{a}_{\parallel} = \hat{b}_{\parallel} \therefore \left(\hat{a} - \hat{b}\right) \cdot \hat{n} = 0$, $\forall \hat{n} \in \Lambda$, thus concluding sufficiency.

To prove necessity, it is assumed that the equality $\hat{a} \cdot \hat{n} = \hat{b} \cdot \hat{n}$ is satisfied, and given that $\|\hat{a}\| = \|\hat{b}\| = 1$, the perpendicular components of $\hat{a}$ and $\hat{b}$ with respect to the rotation axis $\hat{a} \perp \hat{n}, \hat{b} \perp \hat{n}$ can only be located in the circumference described by the intersection of Λ and the

plane perpendicular to $\hat{a}\perp\hat{n}$, that is, the perpendicular components of each vectors $\hat{a}$ and $\hat{b}$ move on the circumference defined by the set

R1Q3

$$\left\{\hat{v}\in\mathbb{R}^3 : \|\hat{v}\|=1, \hat{v}-\hat{n}\times(\hat{n}\times\hat{a})\,cos\,\alpha+(\hat{n}\times\hat{a})sin\,\alpha\ ,\forall\alpha\in\mathbb{R}\right\}$$

$\therefore\ \varpi(\hat{a},\hat{b},\hat{n})$ exists such that, together with axis $\hat{n}$, all the components for the rotation of $\hat{a}$ into $\hat{b}$ exist and are completely defined.

□

Lemma 1 can be used to find the set of all possible axes (and angles) that can be used to rotate an arbitrary unitary vector into another arbitrary unit vector. Remark that the set $\chi(\cdot)$ has an infinite number of components in most cases (notably, when $\hat{a}\neq\hat{b}$), therefore it is often of interest to find only the solution that gives the smallest possible angle. The pair of axis and angle with the lowest possible angle is often unique and will be used as a basis for the desired attitude reference. Lemma 2 provides the way to find this pair.

Lemma 2. Given two normalized and arbitrary vectors $\hat{a},\hat{b}\in\Lambda$ such that $\hat{a}\neq\hat{b}$, the pair of axis and angle $\left\{\hat{n}\in\chi(\hat{a},\hat{b});\varpi(\hat{a},\hat{b},\hat{n})\in\mathbb{R}\right\}$ which gives the lowest possible value of $\varpi(\hat{a},\hat{b},\hat{n})$ is: $\left\{\varpi=arccos\left(\hat{a}\cdot\hat{b}\right);\hat{n}=\dfrac{\hat{a}\times\hat{b}}{sin\varpi}\right\}$.

R1Q3

Proof. First, we take any arbitrary axis $\hat{\eta}\in\chi(\hat{a},\hat{b})$ such that $\hat{\eta}\neq\hat{n}=\frac{\hat{a}\times\hat{b}}{sin\varpi}$. Using this axis, the rotation angle $\varpi(\cdot,\hat{\eta})$ is calculated between the vectors $\hat{a}\perp\hat{\eta}$ and $\hat{b}\perp\hat{\eta}$, which are perpendicular to $\hat{\eta}$.

The proposed shortest angle $\varpi=arccos\,(\hat{a}\cdot\hat{b})$ is the angle between the vectors $\hat{a}$ and $\hat{b}$, and is also the rotation angle associated with the proposed axis $\hat{n}=\frac{\hat{a}\times\hat{b}}{sin\varpi}$. As $\hat{\eta}$ was generated arbitrary and different from $\hat{n}$, if it can be shown that the angle $\varpi(\cdot,\hat{\eta})$ is bigger than the proposed ϖ, then the proof would be complete.

R1Q3

In order to do this, an isosceles triangle ΔE is formed with vectors $\hat{a}$ and $\hat{b}$ and with base of length $\|\hat{a}-\hat{b}\|$. The second isosceles triangle ΔD is formed with vectors $\hat{a}\perp\hat{\eta}$ and $\hat{b}\perp\hat{\eta}$ and also has base of length $\|\hat{a}-\hat{b}\|$. Because ΔE is isosceles and with the same base length as ΔD, ΔE can be projected inside the base of ΔD, which transforms the problem from a 3D perspective into a 2D plane. Therefore, it is a trivial geometric result to prove that $\varpi<\varpi(\cdot,\hat{\eta})$ since $\hat{a}\perp\hat{\eta}<\hat{a}$ and $\hat{b}\perp\hat{\eta}<\hat{b}$, thus concluding the proof. A graphical example can be seen on Figure 2.

□

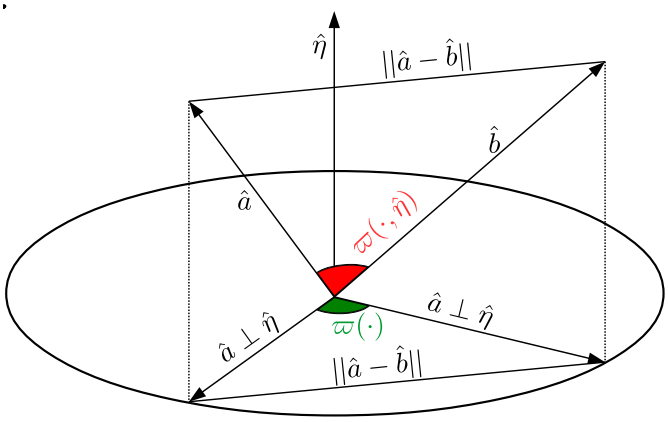

Figure 2.: Shortest axis and angle of rotation between two vectors according to Lemma 2.

On one hand, Lemma 2 allows us to find a unique unit quaternion that represents the attitude, given two normalized vectors $\hat{a}, \hat{b} \in \Lambda$ in different coordinate frames with the smallest possible rotation angle. This quaternion can be described as R1Q3

$$\boldsymbol{q}_f = e^{\frac{\ln\left(\hat{b}\otimes\hat{a}^*\right)}{2}} = cos\,\frac{\varpi}{2} + \hat{n}sin\frac{\varpi}{2} \tag{12}$$

which can be seen as the square root of the unit quaternion $\hat{a}\cdot\hat{b} + \hat{a}\times\hat{b} = cos\,\varpi + \hat{n}sin\varpi$, and where $\hat{a}^* = -\hat{a}$ is the quaternion conjugate of a vector.

On the other hand, Lemma 1 provides the set of all possible attitudes that rotate a reference vector into a desired direction in an axis-angle representation. For our study, this set can be changed into a quaternion attitude set, given a body-fixed normalized vector $\hat{F}_b$ with constant direction and a desired normalized vector in the inertial frame $\hat{F}_d \coloneqq \dfrac{\vec{F}_d}{\|\vec{F}_d\|}$, thus the unique desired quaternion is given by R1Q3

$$\boldsymbol{q}_{f_d} = e^{\frac{\ln\left(\hat{F}_d\otimes\hat{F}_b^*\right)}{2}} = cos\,\frac{\varpi_d}{2} + \hat{n}_d sin\,\frac{\varpi_d}{2} \tag{13}$$

Notice that, the heading of the vehicle is not taken into account, thus, in order to impose a desired heading, we impose

$$\boldsymbol{q}_{\psi_d} = e^{\frac{\psi_d\hat{F}_b}{2}} \tag{14}$$

where ψ_d denotes the desired heading. Finally, it is obvious that the following set

$$Q = \left\{\boldsymbol{q}_d \in \mathbb{H} : \boldsymbol{q}_d = \boldsymbol{q}_{f_d}\otimes\boldsymbol{q}_{\psi_d}, \forall\psi_d \in \mathbb{R}\right\} \tag{15}$$

gives all the possible quaternions that rotate the force from the body frame to the desired direction in the inertial frame. The term ψ_d is considered an independent DoF from the attitude perspective, as it can be changed without affecting the final direction $\hat{F}_d$ of the body vector $\hat{F}_b$.

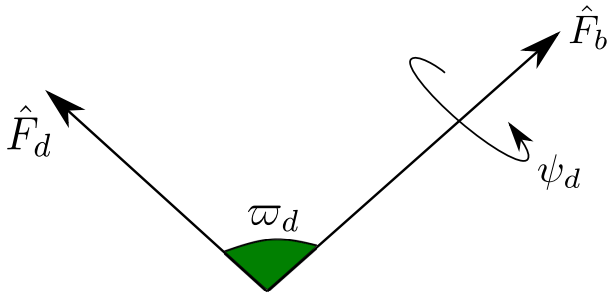

Figure 3.: The relationship between the vectors $\hat{F}_d$ and $\hat{F}_b$, and the angles ϖ_d and ψ_d.

3.2. Derivation of error dynamics

Notice that the desired quaternion is related with errors between vectors, therefore, it is necessary to derive the error dynamics to acquire the equations that will be used to control system (5) – (6).

Define the position error $\vec{p}_e \in \mathbb{R}^3$ as $\vec{p}_e \coloneqq \vec{p} - \vec{p}_d$; then the position tracking objective can be defined as $t \to \infty \implies \vec{p}_e \to \vec{0}$. This implies that $\boldsymbol{q} \otimes \vec{F}_{th} \otimes \boldsymbol{q}^* \to \vec{F}_u$ where $\vec{F}_u$ means the desired thrust obtained from the control algorithm and will be defined later.

Rewriting system (5) in term of errors, it follows that

$$m\,\ddot{\vec{p}}_e = \boldsymbol{q} \otimes \vec{F}_{th} \otimes \boldsymbol{q}^* - \vec{F}_u + m\,\vec{g} + \vec{\zeta}_p \tag{16}$$

Observe that, aerial vehicles cannot generate infinite energy to compensate infinite external perturbations, mainly due to its physical properties. This means that the external perturbations supported by the aerial system can be considered bounded. From our study, the perturbations are considered to be uniform Lipschitz continuous, which also allows for the existence and uniqueness of a solution for the proposed system. Hence, it implies that

$$\left\|\vec{\zeta}_p\right\| \leq L_p \left\| \begin{bmatrix} \vec{p}_e \\ \dot{\vec{p}}_e \end{bmatrix} \right\| \tag{17}$$

For the attitude error dynamics expression, it is first necessary to rewrite (15) in terms of the main thrust in the body frame of the vehicle $\vec{F}_{th}$ and the desired thrust obtained from the control law $\vec{F}_u$ in the inertial frame in the following manner:

$$\boldsymbol{q}_{f_d} \coloneqq e^{\dfrac{\ln\left(\hat{F}_u \otimes \hat{F}_{th}^*\right)}{2}}; \qquad \boldsymbol{q}_{\psi_d} \coloneqq e^{\dfrac{\psi_d \hat{F}_{th}}{2}} \tag{18}$$

The desired angular velocity $\vec{\Omega}_d$ can be obtained by differentiating the desired attitude $\boldsymbol{q}_d \in Q$, as defined in (15), w.r.t. time using quaternion kinematics, $\dot{\boldsymbol{q}} = \dfrac{1}{2}\boldsymbol{q} \otimes \vec{\Omega}$, which results in

$$\begin{aligned} \frac{d}{dt}\boldsymbol{q}_d &= \frac{d}{dt}\left(\boldsymbol{q}_{f_d} \otimes \boldsymbol{q}_{\psi_d}\right) \\ \frac{1}{2}\boldsymbol{q}_d \otimes \vec{\Omega}_d &= \frac{1}{2}\boldsymbol{q}_{f_d} \otimes \vec{\Omega}_{f_d} \otimes \boldsymbol{q}_{\psi_d} + \frac{1}{2}\boldsymbol{q}_{f_d} \otimes \boldsymbol{q}_{\psi_d} \otimes \vec{\Omega}_{\psi_d} \\ \vec{\Omega}_d &= \boldsymbol{q}_{\psi_d}^* \otimes \vec{\Omega}_{f_d} \otimes \boldsymbol{q}_{\psi_d} + \vec{\Omega}_{\psi_d} \end{aligned} \tag{19}$$

where $\vec{\Omega}_d$ is defined in the body frame. The term $\vec{\Omega}_{\psi_d} \coloneqq \dot{\psi}_d\,\hat{F}_{th}$ is defined such that it has the

property

$$\left\|\dot{\vec{\Omega}}_{\psi_d}\right\| \leq L_{\vec{\Omega}_{\psi_d}} \|2 \ln \boldsymbol{q}_e\| \tag{20}$$

for some $L_{\vec{\Omega}_\psi} \in \mathbb{R}_+$ and $\boldsymbol{q}_e \coloneqq \boldsymbol{q}_d^* \otimes \boldsymbol{q}$ defines the quaternion error. $\vec{\Omega}_{f_d}\left(\hat{F}_u, \dot{\hat{F}}_u, \hat{F}_{th}\right) \coloneqq \vec{\Omega}_{f_d}$ can be obtained from the quaternion $\hat{F}_u \otimes \hat{F}_{th}^* = cos\, \varpi_d + \hat{n}_d\, sin\, \varpi_d$ as R1Q3

$$\begin{aligned} \frac{d}{dt}\left(\hat{F}_u \otimes \hat{F}_{th}^*\right) &= \dot{\hat{F}}_u \otimes \hat{F}_{th}^* \\ -\dot{\varpi}\, sin\varpi + \hat{n}\, \dot{\varpi}\, cos\, \varpi &= \dot{\hat{F}}_u \otimes \hat{F}_{th}^* \\ \hat{F}_u \otimes \hat{F}_{th}^* \otimes \vec{\Omega}_{f_d} &= \dot{\hat{F}}_u \otimes \hat{F}_{th}^* \\ \vec{\Omega}_{f_d} &= \hat{F}_{th} \otimes \hat{F}_u^* \otimes \dot{\hat{F}}_u \otimes \hat{F}_{th}^* \end{aligned} \tag{21}$$

An important property of $\vec{\Omega}_d$ is provided in the following theorem.

Theorem 3.1. *The desired angular velocity $\vec{\Omega}_d$ has the property*

$$\left\|\vec{\Omega}_d\right\| \leq L_{\vec{\Omega}_d} \|2 \ln \boldsymbol{q}_e\| \tag{22}$$

for some $L_{\vec{\Omega}_d} \in \mathbb{R}_+$

Proof. First, an expression for $\dot{\hat{F}}_u$ is provided as

$$\dot{\hat{F}}_u = \frac{d}{dt}\frac{\vec{F}_u}{\left\|\vec{F}_u\right\|} = \left(I_3 - \hat{F}_u \hat{F}_u^T\right)\frac{\dot{\vec{F}}_u}{\left\|\vec{F}_u\right\|} \tag{23}$$

A property of matrix $\left(I_3 - \hat{F}_u \hat{F}_u^T\right)$ is $\left(I_3 - \hat{F}_u \hat{F}_u^T\right)\vec{F}_u = \vec{0}$, which can be proven using $\hat{F}_u \hat{F}_u^T \vec{F}_u = \hat{F}_u \left\|\vec{F}_u\right\| = \vec{F}_u$.

The analysis will now focus on the product $\hat{F}_{th} \otimes \hat{F}_u^*$ in equation (21). The vector part of this product can be simplified to R1Q3

$$Vec\left\{\hat{F}_{th} \otimes \hat{F}_u^*\right\} = \hat{F}_u \times \hat{F}_{th} = -\hat{n}_d sin\, \varpi_d \tag{24}$$

which implies that R1Q3

$$\left\|Vec\left\{\hat{F}_{th} \otimes \hat{F}_u^*\right\}\right\| = \|sin\, \varpi_d\| \leq \|2 \ln \boldsymbol{q}_e\| \tag{25}$$

Note 3.2. *The operator $Vec\{\cdot\}$ is defined in* (A5)

From the properties of the quaternion triple product, it can be seen that $\vec{\Omega}_{f_d} \in \mathbb{R}^3$. As the term $\hat{F}_{th} \otimes \hat{F}_u^*$ is multiplying $\vec{\Omega}_{f_d}$, it can be concluded that there exists a constant $L_{\vec{\Omega}_{f_d}}$ such that

$$\left\|\vec{\Omega}_{f_d}\right\| \leq L_{\vec{\Omega}_{f_d}} \|2 \ln \boldsymbol{q}_e\| \tag{26}$$

From property (19), it can be seen that $\vec{\Omega}_d$ has the property described in (22), thus concluding the proof.

□

Differentiating $\vec{\Omega}_d$ w.r.t. time results in

$$\begin{aligned}\dot{\vec{\Omega}}_d = &\quad \boldsymbol{q}^*_{\psi_d} \otimes \dot{\vec{\Omega}}_{f_d} \otimes \boldsymbol{q}_{\psi_d} - \frac{1}{2}\vec{\Omega}_{\psi_d} \otimes \boldsymbol{q}^*_{\psi_d} \otimes \vec{\Omega}_{f_d} \otimes \boldsymbol{q}_{\psi_d} + \frac{1}{2}\boldsymbol{q}^*_{\psi_d} \otimes \vec{\Omega}_{f_d} \otimes \boldsymbol{q}_{\psi_d} \otimes \vec{\Omega}_{\psi_d} + \dot{\vec{\Omega}}_{\psi_d} \\ = &\quad \boldsymbol{q}^*_{\psi_d} \otimes \dot{\vec{\Omega}}_{f_d} \otimes \boldsymbol{q}_{\psi_d} + \left(\boldsymbol{q}^*_{\psi_d} \otimes \vec{\Omega}_{f_d} \otimes \boldsymbol{q}_{\psi_d}\right) \times \vec{\Omega}_{\psi_d} + \dot{\vec{\Omega}}_{\psi_d}\end{aligned} \tag{27}$$

where

$$\dot{\vec{\Omega}}_{f_d} = \hat{F}_{th} \otimes \left(\dot{\hat{F}}^*_u \otimes \dot{\hat{F}}_u + \hat{F}^*_u \otimes \ddot{\hat{F}}_u\right) \otimes \hat{F}^*_{th} \tag{28}$$

From equations (27) and (28), the following theorem can be stated.

Theorem 3.3. *The vector $\dot{\vec{\Omega}}_d$ has the property*

$$\left\|\dot{\vec{\Omega}}_d\right\| \leq L_{\dot{\vec{\Omega}}_d} \left\|2 \ln \boldsymbol{q}_e\right\| \tag{29}$$

for some $L_{\dot{\vec{\Omega}}_d} \in \mathbb{R}_+$

Proof. The first term of (27) ($\boldsymbol{q}^*_{\psi_d} \otimes \dot{\vec{\Omega}}_{f_d} \otimes \boldsymbol{q}_{\psi_d}$) has the property depicted in (29) with the term $\dot{\vec{\Omega}}_{\psi_d}$ and property (20). It can also be concluded that the second term $\left(\boldsymbol{q}^*_{\psi_d} \otimes \vec{\Omega}_{f_d} \otimes \boldsymbol{q}_{\psi_d}\right) \times \vec{\Omega}_{\psi_d}$ also has the property depicted in (29) from Theorem 3.1. This implies that if $\dot{\vec{\Omega}}_{\psi_d}$ in (28) has the property (29), then the proof is complete.

Notice that the term $\dot{\hat{F}}^*_u \otimes \dot{\hat{F}}_u + \hat{F}^*_u \otimes \ddot{\hat{F}}_u$ in (28) has the following property

$$Vec\left\{\dot{\hat{F}}^*_u \otimes \dot{\hat{F}}_u + \hat{F}^*_u \otimes \ddot{\hat{F}}_u\right\} = \overline{0}$$

which implies that the first term in (28) has the property (29).

The second term is multiplied by $\hat{F}_{th} \otimes \hat{F}^*_u$, which was proven to have the property in the proof of Theorem 3.1. Thus, concluding the proof. □

Differentiating the quaternion error w.r.t. time, it follows that

$$\begin{aligned}\dot{\boldsymbol{q}}_e = &\quad = \tfrac{d}{dt}\left(\boldsymbol{q}^*_d \otimes \boldsymbol{q}\right) \\ \frac{1}{2}\boldsymbol{q}_e \otimes \vec{\Omega}_e = &\quad \frac{1}{2}\boldsymbol{q}^*_d \otimes \vec{\Omega}^{\mathcal{I}} \otimes \boldsymbol{q} - \frac{1}{2}\boldsymbol{q}^*_d \otimes \vec{\Omega}^{\mathcal{I}}_d \otimes \boldsymbol{q} \\ \vec{\Omega}_e = &\quad \boldsymbol{q}^* \otimes \left(\vec{\Omega}^{\mathcal{I}} - \vec{\Omega}^{\mathcal{I}}_d\right) \otimes \boldsymbol{q} = \vec{\Omega} - \vec{\Omega}_d\end{aligned} \tag{30}$$

where $\vec{\Omega}^{\mathcal{I}}$ and $\vec{\Omega}^{\mathcal{I}}_d$ are the angular velocity and the desired angular velocity in the inertial frame.

Differentiating $\vec{\Omega}_e$ w.r.t. time results in

$$\dot{\vec{\Omega}}_e = \dot{\vec{\Omega}} - \dot{\vec{\Omega}}_d = J^{-1}\left(\tau - \vec{\Omega} \times J\,\vec{\Omega} + \vec{\zeta}_\Omega\right) - \dot{\vec{\Omega}}_d \tag{31}$$

Equation (31) can be rearranged into

$$J\,\dot{\vec{\Omega}}_e = \quad \tau - \vec{\Omega} \times J\,\vec{\Omega} + \vec{\zeta}_{\Omega_e} \tag{32}$$

where

$$\vec{\zeta}_{\Omega_e} \coloneqq \vec{\zeta}_{\Omega} - J\,\dot{\vec{\Omega}}_d \tag{33}$$

In order to take into account the perturbations present on system (6), and for the existence and uniqueness of the solution for $\dot{\vec{\Omega}}_e$ in (32), it is assumed that this perturbation is uniform Lipschitz continuous, which implies that it has the property

$$\left\|\vec{\zeta}_{\Omega}\right\| \leq L_{\vec{\zeta}_{\Omega}} \left\| \begin{bmatrix} 2\,\ln \boldsymbol{q}_e \\ \Omega_e \end{bmatrix} \right\| \tag{34}$$

It can be seen that $\vec{\zeta}_{\Omega_e}$ has a similar property

$$\left\|\vec{\zeta}_{\Omega_e}\right\| \leq L_{\vec{\zeta}_{\Omega_e}} \left\| \begin{bmatrix} 2\,\ln \boldsymbol{q}_e \\ \Omega_e \end{bmatrix} \right\| \tag{35}$$

for some $L_{\vec{\zeta}_{\Omega_e}} \in \mathbb{R}_+$. This can be proven from properties (29) and (34).

3.3. Virtual fully actuated mathematical model

Theorem 3.4. *Let there be two independent control laws $\vec{F}_u \in \mathbb{R}^3$ and $\vec{\tau} \in \mathbb{R}^3$ stabilizing the following fully actuated system*

$$\mathcal{H}_a : \begin{cases} m\,\ddot{\vec{p}}_e &= \vec{F}_u + m\,\vec{g} + \vec{\zeta}_p \\ J\,\dot{\vec{\Omega}}_e &= \vec{\tau}\ - \vec{\Omega} \times J\,\vec{\Omega} + \vec{\zeta}_{\Omega_e} \end{cases} \tag{36}$$

along with their Lyapunov candidate functions

$$V_{p_e} = f\left(\dot{\vec{p}}_e, \vec{p}_e\right) : \mathbb{R}^6 \to \mathbb{R}_+ \qquad \textit{with} \qquad \dot{V}_{p_e} \leq 0 \tag{37}$$

$$V_{q_e} = g\left(\boldsymbol{q}_e, \vec{\Omega}_e\right) : \begin{bmatrix} \mathbb{H} \\ \mathbb{R}^3 \end{bmatrix} \to \mathbb{R}_+ \quad \textit{with} \qquad \dot{V}_{q_e} \leq 0 \tag{38}$$

Therefore, if condition

$$\begin{aligned} \frac{\partial\, g\left(\boldsymbol{q}_e, \vec{\Omega}_e\right)}{\partial \vec{\Omega}_e}\, J^{-1}\left(\vec{\tau} - \vec{\Omega} \times J\,\vec{\Omega}\right) \leq\ & -\left[\left\| \frac{\partial\, g\left(\boldsymbol{q}_e, \vec{\Omega}_e\right)}{\partial \vec{\Omega}_e} \right\| \left\| J^{-1} \right\| L_{\vec{\zeta}_{\Omega_e}} + \right. \\ & \frac{1}{2}\left\| \frac{\partial\, g\left(\boldsymbol{q}_e, \vec{\Omega}_e\right)}{\partial \boldsymbol{q}_e} \right\| \left\| \vec{\Omega}_e \right\| - \left[\left\| \frac{\partial\, g\left(\boldsymbol{q}_e, \vec{\Omega}_e\right)}{\partial \vec{\Omega}_e} \right\| \left\| J^{-1} \right\| L_{\vec{\zeta}_{\Omega_e}} + \\ & \left. \left\| \sum_i f_i \right\| \left\| \frac{\partial\, f\left(\dot{\vec{p}}_e, \vec{p}_e\right)}{\partial \dot{\vec{p}}_e} \right\| \right] \left\| 2\,\ln \boldsymbol{q}_e \right\| \end{aligned} \tag{39}$$

is satisfied, then

$$\begin{bmatrix} p_e \\ \dot{p}_e \\ \psi - \psi_d \end{bmatrix} = \vec{0} \tag{40}$$

for some desired $\psi_d \in \mathbb{R}$. This implies that $\boldsymbol{q} \otimes \vec{F}_{th} \otimes \boldsymbol{q}^* \to \vec{F}_u$ signifying that $\sum_i f_i = \left\|\vec{F}_u\right\|$, hence controllers $\vec{F}_u$ and $\vec{\tau}$ also stabilizes system (5) *and* (6).

Proof. Define the following Lyapunov candidate function for the rigid body system (16) and (32) as

$$V\left(\dot{\vec{p}}_e, \vec{p}_e, \boldsymbol{q}_e, \vec{\Omega}_e\right) = f\left(\dot{\vec{p}}_e, \vec{p}_e\right) + g\left(\boldsymbol{q}_e, \vec{\Omega}_e\right) \tag{41}$$

Differentiating the above w.r.t. time results in

$$\begin{aligned}\dot{V}\left(\dot{\vec{p}}_e, \vec{p}_e, \boldsymbol{q}_e, \vec{\Omega}_e\right) = & \left[\begin{array}{cc} \dfrac{\partial f\left(\dot{\vec{p}}_e, \vec{p}_e\right)}{\partial \vec{p}_e} & \dfrac{\partial f\left(\dot{\vec{p}}_e, \vec{p}_e\right)}{\partial \dot{\vec{p}}_e} \end{array}\right]\left[\begin{array}{c} \dot{\vec{p}}_e \\ \boldsymbol{q} \otimes \vec{F}_{th} \otimes \boldsymbol{q}^* + \vec{g} + \vec{\zeta}_p \end{array}\right] + \\ & \left[\begin{array}{cc} \dfrac{\partial g\left(\boldsymbol{q}_e, \vec{\Omega}_e\right)}{\partial \boldsymbol{q}_e} & \dfrac{\partial g\left(\boldsymbol{q}_e, \vec{\Omega}_e\right)}{\partial \vec{\Omega}_e} \end{array}\right]\left[\begin{array}{c} \dfrac{1}{2}\boldsymbol{q}_e \otimes \vec{\Omega}_e \\ J^{-1}\left(\vec{\tau} - \vec{\Omega} \times J\,\vec{\Omega} + \vec{\zeta}_{\Omega_e}\right) \end{array}\right]\end{aligned} \tag{42}$$

Adding the term $\dfrac{\partial f\left(\dot{\vec{p}}_e, \vec{p}_e\right)}{\partial \dot{\vec{p}}_e}\left(\vec{F}_u - \vec{F}_u\right) = 0$ to (42) yields

$$\begin{aligned}\dot{V}\left(\dot{\vec{p}}_e, \vec{p}_e, \boldsymbol{q}_e, \vec{\Omega}_e\right) = & \left[\begin{array}{cc} \dfrac{\partial f\left(\dot{\vec{p}}_e, \vec{p}_e\right)}{\partial \vec{p}_e} & \dfrac{\partial f\left(\dot{\vec{p}}_e, \vec{p}_e\right)}{\partial \dot{\vec{p}}_e} \end{array}\right]\left[\begin{array}{c} \dot{\vec{p}}_e \\ \vec{F}_u + \vec{g} + \vec{\zeta}_p \end{array}\right] + \\ & \frac{\partial f\left(\dot{\vec{p}}_e, \vec{p}_e\right)}{\partial \dot{\vec{p}}_e}\left(\boldsymbol{q} \otimes \vec{F}_{th} \otimes \boldsymbol{q}^* - \vec{F}_u\right) + \\ & \left[\begin{array}{cc} \dfrac{\partial g\left(\boldsymbol{q}_e, \vec{\Omega}_e\right)}{\partial \boldsymbol{q}_e} & \dfrac{\partial g\left(\boldsymbol{q}_e, \vec{\Omega}_e\right)}{\partial \vec{\Omega}_e} \end{array}\right]\left[\begin{array}{c} \dfrac{1}{2}\boldsymbol{q}_e \otimes \vec{\Omega}_e \\ J^{-1}\left(\vec{\tau} - \vec{\Omega} \times J\,\vec{\Omega} + \vec{\zeta}_{\Omega_e}\right) \end{array}\right]\end{aligned} \tag{43}$$

Notice that $\vec{F}_u$ is defined to stabilize the translational system in (36) implying that the first part of (43) is negative semi-definite. Then

$$\begin{aligned}\dot{V}\left(\dot{\vec{p}}_e, \vec{p}_e, \boldsymbol{q}_e, \vec{\Omega}_e\right) \leq & \frac{\partial f\left(\dot{\vec{p}}_e, \vec{p}_e\right)}{\partial \dot{\vec{p}}_e}\left(\boldsymbol{q} \otimes \vec{F}_{th} \otimes \boldsymbol{q}^* - \vec{F}_u\right) + \\ & \left[\begin{array}{cc} \dfrac{\partial g\left(\boldsymbol{q}_e, \vec{\Omega}_e\right)}{\partial \boldsymbol{q}_e} & \dfrac{\partial g\left(\boldsymbol{q}_e, \vec{\Omega}_e\right)}{\partial \vec{\Omega}_e} \end{array}\right]\left[\begin{array}{c} \dfrac{1}{2}\boldsymbol{q}_e \otimes \vec{\Omega}_e \\ J^{-1}\left(\vec{\tau} - \vec{\Omega} \times J\,\vec{\Omega} + \vec{\zeta}_{\Omega_e}\right) \end{array}\right]\end{aligned} \tag{44}$$

The term $\dfrac{\partial f\left(\dot{\vec{p}}_e, \vec{p}_e\right)}{\partial \dot{\vec{p}}_e}\left(\boldsymbol{q} \otimes \vec{F}_{th} \otimes \boldsymbol{q}^* - \vec{F}_u\right)$ can be further simplified by taking into account that the length of the error vector $\boldsymbol{q} \otimes \vec{F}_{th} \otimes \boldsymbol{q}^* - \vec{F}_u$ is less than the length of the arc made between the two vectors, that is

$$\left\|\boldsymbol{q} \otimes \vec{F}_{th} \otimes \boldsymbol{q}^* - \vec{F}_u\right\| \leq \left\|\varpi_d \sum_i f_i\right\| \leq \|2\,\ln \boldsymbol{q}_e\| \left\|\sum_i f_i\right\| \tag{45}$$

Substituting this inequality into (44) results in

$$\begin{aligned}\dot{V}\left(\dot{\vec{p}}_e,\vec{p}_e,\boldsymbol{q}_e,\vec{\Omega}_e\right) \leq\ & \tfrac{1}{2}\frac{\partial g\left(\boldsymbol{q}_e,\vec{\Omega}_e\right)}{\partial \boldsymbol{q}_e}\left(\boldsymbol{q}\otimes\vec{\Omega}_e\right)+\frac{\partial g\left(\boldsymbol{q}_e,\vec{\Omega}_e\right)}{\partial \vec{\Omega}_e}J^{-1}\left(\vec{\tau}-\vec{\Omega}\times J\,\vec{\Omega}+\vec{\zeta}_{\Omega_e}\right)+\\ & \left\|\sum_i f_i\right\|\left\|\frac{\partial f\left(\dot{\vec{p}}_e,\vec{p}_e\right)}{\partial \dot{\vec{p}}_e}\right\|\|2\,\ln \boldsymbol{q}_e\|\\ =\ & \tfrac{1}{2}\frac{\partial g\left(\boldsymbol{q}_e,\vec{\Omega}_e\right)}{\partial \boldsymbol{q}_e}\left(\boldsymbol{q}\otimes\vec{\Omega}_e\right)+\frac{\partial g\left(\boldsymbol{q}_e,\vec{\Omega}_e\right)}{\partial \vec{\Omega}_e}J^{-1}\left(\vec{\tau}-\vec{\Omega}\times J\,\vec{\Omega}\right)+\\ & \frac{\partial g\left(\boldsymbol{q}_e,\vec{\Omega}_e\right)}{\partial \vec{\Omega}_e}J^{-1}\,\zeta_{\Omega_e}+\left\|\sum_i f_i\right\|\left\|\frac{\partial f\left(\dot{\vec{p}}_e,\vec{p}_e\right)}{\partial \dot{\vec{p}}_e}\right\|\|2\,\ln \boldsymbol{q}_e\|\end{aligned} \tag{46}$$

Using property (35), and the fact that $\boldsymbol{q}$ is a unitary quaternion, equation (46) can be rewritten as

$$\begin{aligned}\dot{V}\left(\dot{\vec{p}}_e,\vec{p}_e,\boldsymbol{q}_e,\vec{\Omega}_e\right) \leq\ & \left\|\frac{\partial g\left(\boldsymbol{q}_e,\vec{\Omega}_e\right)}{\partial \boldsymbol{q}_e}\right\|\left\|\frac{\vec{\Omega}_e}{2}\right\|+\frac{\partial g\left(\boldsymbol{q}_e,\vec{\Omega}_e\right)}{\partial \vec{\Omega}_e}J^{-1}\left(\vec{\tau}-\vec{\Omega}\times J\vec{\Omega}\right)+\\ & \left\|\frac{\partial g\left(\boldsymbol{q}_e,\vec{\Omega}_e\right)}{\partial \vec{\Omega}_e}\right\|\left\|J^{-1}\right\|L_{\vec{\zeta}_{\Omega_e}}\left\|\begin{bmatrix}2\ln \boldsymbol{q}_e\\ \Omega_e\end{bmatrix}\right\|+\left\|\sum_i f_i\right\|\left\|\frac{\partial f\left(\dot{\vec{p}}_e,\vec{p}_e\right)}{\partial \dot{\vec{p}}_e}\right\|\|2\ln \boldsymbol{q}_e\|\\ \leq\ & \frac{\partial g\left(\boldsymbol{q}_e,\vec{\Omega}_e\right)}{\partial \vec{\Omega}_e}J^{-1}\left(\vec{\tau}-\vec{\Omega}\times J\vec{\Omega}\right)+\\ & \left[\left\|\frac{\partial g\left(\boldsymbol{q}_e,\vec{\Omega}_e\right)}{\partial \vec{\Omega}_e}\right\|\left\|J^{-1}\right\|L_{\vec{\zeta}_{\Omega_e}}+\left\|\sum_i f_i\right\|\left\|\frac{\partial f\left(\dot{\vec{p}}_e,\vec{p}_e\right)}{\partial \dot{\vec{p}}_e}\right\|\right]\|2\ln \boldsymbol{q}_e\|+\\ & \left[\left\|\frac{\partial g\left(\boldsymbol{q}_e,\vec{\Omega}_e\right)}{\partial \vec{\Omega}_e}\right\|\left\|J^{-1}\right\|L_{\vec{\zeta}_{\Omega_e}}+\tfrac{1}{2}\left\|\frac{\partial g\left(\boldsymbol{q}_e,\vec{\Omega}_e\right)}{\partial \boldsymbol{q}_e}\right\|\right]\left\|\vec{\Omega}_e\right\|\end{aligned} \tag{47}$$

According to inequality (47), in order to ensure that $\dot{V}\left(\dot{\vec{p}}_e,\vec{p}_e,\boldsymbol{q}_e,\vec{\Omega}_e\right)\leq 0$, the condition (39) must be met, thus concluding the proof.

□

4. Control design methodology

The algorithm to obtain the equivalent control law for the under actuated system from the control scheme of the virtual fully actuated system is obtained as a direct result of Theorem 3.4 and can be seen in Algorithm 1.

Three classical controllers are described and used to control the aerial vehicle using the model given in (36). The stability of each controller is ensured using Theorem 3.4.

4.1. State-feedback control

The most straightforward control methodology is to use a feedback of the state vector as a control input.

Propose the following Lyapunov candidates functions

$$V_{p_e} = f\left(\dot{\vec{p}}_e,\vec{p}_e\right)=\overline{x}_p^T\,P_p\,\overline{x}_p \tag{48}$$

$$V_{q_e} = g\left(\vec{\Omega}_e,\boldsymbol{q}_e\right)=\overline{x}_\Omega^T\,P_\Omega\,\overline{x}_\Omega \tag{49}$$

with $\overline{x}_p \coloneqq \begin{bmatrix}\vec{p}_e^T & \dot{\vec{p}}_e^T\end{bmatrix}^T$ and $\overline{x}_\Omega \coloneqq \begin{bmatrix}(2\ln \boldsymbol{q}_e)^T & \vec{\Omega}_e^T\end{bmatrix}^T$ and P_p, P_Ω are positive real symmetric matrices of appropriate dimensions.

Algorithm 1 The control design methodology

Input: $\vec{F}_u\left(\dot{\vec{p}}_e, \vec{p}_e\right)$, $\vec{\tau}\left(\boldsymbol{q}, \vec{\Omega}\right)$, V_{p_e}, V_{q_e}, ψ_d, $\dot{\psi}_d$ ▷ See system (36) and definitions (37) and (38)

Ensure: Condition (39), $\dot{V}_{p_e} \leq 0$, $\dot{V}_{q_e} < 0$ ▷ See definitions (37) and (38)

$\boldsymbol{q}_{f_d} \leftarrow e^{\frac{\ln\left(\hat{F}_u \otimes \hat{F}_b^*\right)}{2}}$ ▷ See definition (13)

$\boldsymbol{q}_{\psi_d} \leftarrow e^{\frac{\psi_d \hat{F}_b}{2}}$ ▷ See definition (14)

$\boldsymbol{q}_d \leftarrow \boldsymbol{q}_{f_d} \otimes \boldsymbol{q}_{\psi_d}$ ▷ See set (15)

$\boldsymbol{q}_e \leftarrow \boldsymbol{q}_d^* \otimes \boldsymbol{q}$ ▷ See (20)

$\vec{\Omega}_{\psi_d} \leftarrow \dot{\psi}_d \hat{F}_{th}$ ▷ See (19)

$\vec{\Omega}_d \leftarrow \boldsymbol{q}_{\psi_d}^* \otimes \vec{\Omega}_{f_d} \otimes \boldsymbol{q}_{\psi_d} + \vec{\Omega}_{\psi_d}$ ▷ See (19)

$\vec{\Omega}_e \leftarrow \vec{\Omega} - \vec{\Omega}_d$ ▷ See (30)

$\sum_i f_i \leftarrow \left\|\vec{F}_u\right\|$ ▷ See definition (7)

$\vec{\tau} \leftarrow \vec{\tau}\left(\boldsymbol{q}_e, \vec{\Omega}_e\right)$ ▷ See system (2)

Output: $\sum_i f_i$, $\vec{\tau}\left(\boldsymbol{q}_e, \vec{\Omega}_e\right)$ ▷ These are the control inputs of systems (6) and (7)

Differentiating (48) w.r.t. time results in

$$\dot{V}_{p_e} = \frac{\partial f(\bar{x}_p)}{\partial \bar{x}_p} \begin{bmatrix} \dot{\vec{p}}_e \\ \frac{\vec{F}_u}{m} + \vec{g} + \frac{\vec{\zeta}_p}{m} \end{bmatrix} \tag{50}$$

Proposing

$$\vec{F}_u = -m\, K_{pt}\, \vec{p}_e - m\, K_{dt}\, \dot{\vec{p}}_e - m\vec{g}, \tag{51}$$

Then,

$$\begin{aligned} \dot{V}_{p_e} = & \frac{\partial f(\bar{x}_p)}{\partial \bar{x}_p} \begin{bmatrix} \dot{\vec{p}}_e \\ -K_{pt}\, \vec{p}_e - K_{dt}\, \dot{\vec{p}}_e + \frac{\vec{\zeta}_p}{m} \end{bmatrix} \\ = & \bar{x}_p^T \left(\begin{bmatrix} \vec{0} & -K_{pt} \\ I_{3\times 3} & -K_{dt} \end{bmatrix} P_p + P_p \begin{bmatrix} \vec{0} & I_{3\times 3} \\ -K_{pt} & -K_{dt} \end{bmatrix} \right) \bar{x}_p + \frac{\partial f(\bar{x}_p)}{\partial \dot{\vec{p}}_e} \frac{\vec{\zeta}_p}{m} \end{aligned} \tag{52}$$

Gain matrices $K_{pt}, K_{dt} \in \mathbb{R}^{3\times 3}$ are chosen such that

$$\begin{bmatrix} \vec{0} & -K_{pt} \\ I_{3\times 3} & -K_{dt} \end{bmatrix} P_p + P_p \begin{bmatrix} \vec{0} & I_{3\times 3} \\ -K_{pt} & -K_{dt} \end{bmatrix} = -Q_p \tag{53}$$

with $Q_p > 0$. Therefore

$$\dot{V}_{p_e} = -\bar{x}_p^T\, Q_p\, \bar{x}_p + \frac{\partial f(\bar{x}_p)}{\partial \dot{\vec{p}}_e} \frac{\vec{\zeta}_p}{m} \tag{54}$$

From (17), it follows that

R1Q2

$$\dot{V}_{p_e} \leq \quad -\|Q_p\|\,\|\overline{x}_p\|^2 + \|P_p\|\,\frac{L_p}{m}\,\|\overline{x}_p\|^2 = -\left[\|Q_p\| - \|P_p\|\,\frac{L_p}{m}\right]\,\|\overline{x}_p\|^2 \tag{55}$$

which implies that $\dot{f}\left(\dot{\vec{p}}_e, \vec{p}_e\right) \leq 0$ if $\|Q_p\| > \|P_p\|\,\dfrac{L_p}{m}$.

A similar analysis can be made for the attitude dynamics with function (49) without any loss of generality using the controller

$$\vec{\tau} = J\left[-K_{p\vartheta}\,(2\,\ln \boldsymbol{q}_e) - K_{d\vartheta}\,\vec{\Omega}_e\right] + \vec{\Omega} \times J\vec{\Omega}, \tag{56}$$

and the following Lyapunov candidate function

$$\begin{bmatrix} \vec{0} & -K_{p\vartheta} \\ I_{3\times 3} & -K_{d\vartheta} \end{bmatrix} P_\Omega + P_\Omega \begin{bmatrix} \vec{0} & I_{3\times 3} \\ -K_{p\vartheta} & -K_{d\vartheta} \end{bmatrix} = -Q_\Omega \tag{57}$$

with $Q_\Omega > 0$ and with gain matrices $K_{p\vartheta}, K_{d\vartheta} \in \mathbb{R}^{3\times 3}$ chosen properly for holding the equality. Therefore, this results in

$$\dot{g}\left(\vec{\Omega}_e, \boldsymbol{q}_e\right) \leq -\left[\|Q_\Omega\| - \|P_\Omega\|\,\left\|J^{-1}\right\|\,L_{\vec{\zeta}_{\Omega_e}}\right]\,\|\overline{x}_\Omega\|^2 \tag{58}$$

which implies that $\dot{g}\left(\vec{\Omega}_e, \boldsymbol{q}_e\right) \leq 0$ if $\|Q_\Omega\| > \|P_\Omega\|\,\left\|J^{-1}\right\|\,L_{\vec{\zeta}_{\Omega_e}}$.

Analysis of condition (39)

It has been proven that the proposed control laws stabilize system (36). Following the design scheme in Theorem 3.4, the inequality (39) will be analyzed for the proposed control laws in order to determine asymptotic stability.

Substituting (51) into (39) results in

$$\begin{aligned} -\|P_\Omega\|\,\left\|\vec{\Omega}_e\right\|\,\left(\|K_{p\vartheta}\|\,\|2\ln \boldsymbol{q}_e\| + \|K_{d\vartheta}\|\,\left\|\vec{\Omega}_e\right\|\right) \leq \quad & -\left[\|P_\Omega\|\,\left\|\vec{\Omega}_e\right\|\,\left\|J^{-1}\right\|\,L_{\vec{\zeta}_{\Omega_e}} + \right. \\ & \left.\frac{1}{2}\,\|P_\Omega\|\,\|2\ln \boldsymbol{q}_e\|\right]\,\left\|\vec{\Omega}_e\right\| - \\ & \left[\|P_\Omega\|\,\left\|\vec{\Omega}_e\right\|\,\left\|J^{-1}\right\|\,L_{\vec{\zeta}_{\Omega_e}} + \right. \\ & \left.\|P_p\|\,\left\|\dot{\vec{p}}_e\right\|\,\left\|\sum_i f_i\right\|\right]\,\|2\ln \boldsymbol{q}_e\| \end{aligned} \tag{59}$$

The analysis can be simplified by splitting and regrouping the terms in (59) based on terms depending on $\|2\,\ln \boldsymbol{q}_e\|$ and others depending solely on $\left\|\vec{\Omega}_e\right\|$. On one hand, the terms depending on $\|2\,\ln \boldsymbol{q}_e\|$ are grouped in the following inequality

$$\begin{aligned} -\|P_\Omega\|\,\left\|\vec{\Omega}_e\right\|\,\|K_{p\vartheta}\|\,\|2\,\ln \boldsymbol{q}_e\| \leq \quad & -\left(\left\|J^{-1}\right\|\,L_{\vec{\zeta}_{\Omega_e}} + \tfrac{1}{2}\right)\,\|P_\Omega\|\,\left\|\vec{\Omega}_e\right\|\,\|2\,\ln \boldsymbol{q}_e\| \\ & -\|P_p\|\,\left\|\dot{\vec{p}}_e\right\|\,\left\|\sum_i f_i\right\|\,\|2\,\ln \boldsymbol{q}_e\| \\ \Longrightarrow \qquad -\|P_\Omega\|\,\left\|\vec{\Omega}_e\right\|\,\|K_{p\vartheta}\| \leq \quad & -\left(\left\|J^{-1}\right\|\,L_{\vec{\zeta}_{\Omega_e}} + \tfrac{1}{2}\right)\,\|P_\Omega\|\,\left\|\vec{\Omega}_e\right\| \\ & -\|P_p\|\,\left\|\dot{\vec{p}}_e\right\|\,\left\|\sum_i f_i\right\| \\ \Longrightarrow \qquad \|K_{p\vartheta}\| \geq \quad & \left\|J^{-1}\right\|\,L_{\vec{\zeta}_{\Omega_e}} + \tfrac{1}{2} + \frac{\|P_p\|\left\|\dot{\vec{p}}_e\right\|\left\|\sum_i f_i\right\|}{\|P_\Omega\|\,\left\|\vec{\Omega}_e\right\|} \end{aligned} \tag{60}$$

In this case, the effect produced by the coupled dynamics on the stability of the system is mainly presented in the last term of (60), which can be defined as

$$\epsilon_\vartheta \coloneqq \frac{\|P_p\| \left\|\dot{\vec{p}}_e\right\| \left\|\sum_i f_i\right\|}{\|P_\Omega\| \left\|\vec{\Omega}_e\right\|} \tag{61}$$

and depends on the vehicles thrust force and the velocity dynamics.

Substituting ϵ_ϑ into (60) yields

$$\|K_{p\vartheta}\| \geq \left\|J^{-1}\right\| L_{\vec{\zeta}_{\Omega_e}} + \frac{1}{2} + \epsilon_\vartheta \tag{62}$$

Observe that, if $\|P_\Omega\| >> \|P_p\|$, then $\epsilon_\vartheta \approx 0$, which makes its effect negligible. Therefore, the condition is met if $K_{p\vartheta}$ is chosen such that (62) is enforced.

On the other hand, the terms from (59) that depend solely on $\left\|\vec{\Omega}_e\right\|$ can be grouped as

$$\begin{aligned} -\|P_\Omega\| \left\|\vec{\Omega}_e\right\|^2 \|K_{d\vartheta}\| &\leq -\|P_\Omega\| \left\|\vec{\Omega}_e\right\|^2 \left\|J^{-1}\right\| L_{\vec{\zeta}_{\Omega_e}} \\ \implies \|K_{d\vartheta}\| &\geq \left\|J^{-1}\right\| L_{\vec{\zeta}_{\Omega_e}} \end{aligned} \tag{63}$$

If $K_{d\vartheta}$ is chosen in order to enforce (63), it can be concluded that system (5) - (6) is asymptotically stable to the equilibrium point (40) with control inputs $\vec{F}_u$ and $\vec{\tau}$.

For this controller, the stability was proven in the presence of perturbations with some conditions to hold. However, the disadvantage of using a state feedback controller is that the variable ϵ_ϑ could make the system unstable under certain conditions. The condition $\epsilon_\vartheta \approx 0$ can be ensured by limiting the initial conditions of the system. This in turn limits the stability to be local rather than global.

4.2. Energy shaping controller

Energy shaping is a technique that is closely associated with the control of kinematic chains, like robotic arms. The premise is to change the dynamics of the system in order to have a different mechanical impedance. The main objective of the proposed controller is to change the potential energy of the system in order to mitigate the effects that the couple dynamics have on the system. The fundamentals and a more thorough description of this type of control can be found in Brogliato et al. (2007).

The Lyapunov candidate functions can be proposed as the total energy of the translation and attitude systems, respectively. An additional term is added in order to change the location of the global minimum of the potential energy. R1Q3

$$V_{p_e} = \frac{m\,\dot{\vec{p}}_e^{\,T}\,\dot{\vec{p}}_e}{2} + K_{pt} \log\left(cosh\vec{p}_e\right) \tag{64}$$

$$V_{q_e} = \frac{\vec{\Omega}_e^T\, J\, \vec{\Omega}_e}{2} + \phi\left(\boldsymbol{q}_e\right) - \phi_{min} \tag{65}$$

The terms $K_{pt} \log\left(cosh\vec{p}_e\right) > 0$ and $\phi\left(\boldsymbol{q}_e\right) - \phi_{min} > 0$ describe the desired shape of the new potential energy imposed to system (36). $\phi_{min} \in \mathbb{R}$ is a constant term such that $\phi\left(1\right) = \phi_{min}$ and K_{pt} is a gain matrix. $\phi\left(\boldsymbol{q}_e\right) : \mathbb{H} \to \mathbb{R}^3$ is defined such that

$$\frac{\partial \phi\left(\boldsymbol{q}_e\right)}{\partial\left(2\,\ln \boldsymbol{q}_e\right)} = K_{p\vartheta}\, sinh\left(2\,\ln \boldsymbol{q}_e\right) - \vec{\zeta}_{\vartheta_e} \tag{66}$$

A useful property of $\phi\left(\boldsymbol{q}_e\right)$ is that it is convex and has only one minimum. This can be seen from the fact that $\left\|K_{p\vartheta}\, sinh\left(2\,\ln \boldsymbol{q}_e\right)\right\| \geq L_{\vec{\zeta}_{\Omega_e}} \left\|(2\,\ln \boldsymbol{q}_e)\right\|$ and R1Q3

$$\frac{\partial^2 \phi\left(\boldsymbol{q}_e\right)}{\partial\left(2\,\ln \boldsymbol{q}_e\right)^2} \geq K_{p\vartheta} cosh(2\,\ln \boldsymbol{q}_e) - L_{\vec{\zeta}_{\Omega_e}} > 0 \tag{67}$$

with the assumption that $\vec{\zeta}_{\vartheta_e}$ is assumed to be Lipschitz continuous on the state $(2\,\ln \boldsymbol{q}_e)$ and $K_{p\vartheta}$ is a gain matrix.

Note 4.1. *This type of controller uses what is known as energy storage functions as shown in* (64) *and* (65)*, which are functions that can calculate the amount of energy a system has. In this context, energy can be associated with real physical parameters like kinetic or potential energy, or it can be seen as an objective form to measure a control goal.*

These energy storage functions normally have relatively few restrictions, like being positive and convex. In our case, hyperbolic functions were chosen because they meet these two properties while returning relatively big values when the system is far from its desired state. This allows the control to exhibit an aggressive nonlinear behavior the further away the system is to the reference, but its effects are mild if the errors are small.

Differentiating (64) w.r.t. time yields

$$\dot{V}_{p_e} = m\dot{\vec{p}}_e^{\,T}\ddot{\vec{p}}_e + \left(K_{pt}\,\tanh \vec{p}_e\right)^T \dot{\vec{p}}_e$$

Propose

$$\vec{F}_u = m\,\vec{g} - K_{dt}\,\dot{\vec{p}}_e - K_{pt}\,\tanh \vec{p}_e \tag{68}$$

then

$$\begin{aligned} \dot{V}_{p_e} &= \dot{\vec{p}}_e^{\,T}\left[-K_{dt}\,\dot{\vec{p}}_e - K_{pt}\,\tanh \vec{p}_e + \vec{\zeta}_p\right] + \left(K_{pt}\,\tanh \vec{p}_e\right)^T \dot{\vec{p}}_e \\ &= \dot{\vec{p}}_e^{\,T}\left(-K_{dt}\,\dot{\vec{p}}_e + \vec{\zeta}_p\right). \end{aligned} \tag{69}$$

Consider that perturbation into the translation system depends only on the velocity error as

$$\left\|\vec{\zeta}_p\right\| \leq L_p \left\|\dot{\vec{p}}_e\right\| \tag{70}$$

Thus, (69) can be simplified into

$$\dot{V}_{p_e} \leq -\left(\|K_{dt}\| - L_p\right) \left\|\dot{\vec{p}}_e\right\|^2 \leq 0 \tag{71}$$

Using the Krasovskii-LaSalle's invariant set theorem, the translational system equations in (36) and property (70), it can be concluded that the largest invariant set occurs when $\vec{F}_u = -m\,\vec{g}$, which implies that the translation system in (36) is asymptotically stable if $\|K_{dt}\| > L_p$.

Differentiating (65) w.r.t. time results in

$$\dot{V}_{q_e} = \vec{\Omega}_e^T J \dot{\vec{\Omega}}_e + \frac{\partial\, \phi\left(\boldsymbol{q}_e\right)}{\partial\, \left(2\, \ln \boldsymbol{q}_e\right)}^T \vec{\Omega}_e \tag{72}$$

Propose R1Q3

$$\vec{\tau} = \vec{\Omega} \times J\, \vec{\Omega} - K_{d\vartheta}\, \vec{\Omega}_e - K_{p\vartheta}\, sinh\left(2\, \ln \boldsymbol{q}_e\right). \tag{73}$$

Then R1Q3

$$\begin{aligned} \dot{V}_{q_e} = & \vec{\Omega}_e^T \left[-K_{d\vartheta}\, \vec{\Omega}_e - K_{p\vartheta}\, sinh\left(2\, \ln \boldsymbol{q}_e\right) + \vec{\zeta}_{\Omega_e}\right] + \frac{\partial\, \phi(\boldsymbol{q}_e)}{\partial (2\, \ln \boldsymbol{q}_e)}^T \vec{\Omega}_e \\ = & \vec{\Omega}_e^T \left[-K_{d\vartheta}\, \vec{\Omega}_e - K_{p\vartheta}\, sinh\left(2\, \ln \boldsymbol{q}_e\right) + \right. \\ & \left. \vec{\zeta}_{\dot{\vartheta}_e} + \vec{\zeta}_{\vartheta_e}\right] + \left[K_{p\vartheta}\, sinh\left(2\, \ln \boldsymbol{q}_e\right) - \vec{\zeta}_{\vartheta_e}\right]^T \vec{\Omega}_e \\ = & \vec{\Omega}_e^T \left[-K_{d\vartheta}\, \vec{\Omega}_e + \vec{\zeta}_{\dot{\vartheta}_e}\right] \end{aligned} \tag{74}$$

Let us assume from (35) that the effects of the perturbation $\vec{\zeta}_{\Omega_e}$ can be separated as $\vec{\zeta}_{\Omega_e} = \vec{\zeta}_{\dot{\vartheta}_e} + \vec{\zeta}_{\vartheta_e}$, then

$$\left\|\vec{\zeta}_{\vartheta_e}\right\| \leq L_{\vec{\zeta}_{\Omega_e}} \left\|2\, \ln \boldsymbol{q}_e\right\| \tag{75}$$

and

$$\left\|\vec{\zeta}_{\dot{\vartheta}_e}\right\| \leq L_{\vec{\zeta}_{\Omega_e}} \left\|\vec{\Omega}_e\right\| \tag{76}$$

Therefore (74) becomes

$$\dot{V}_{q_e} \leq -\left(\|K_{d\vartheta}\| - L_{\vec{\zeta}_{\Omega_e}}\right) \left\|\vec{\Omega}_e\right\|^2 \leq 0 \tag{77}$$

Using the Krasovskii-LaSalle's invariant set theorem, the rotational system equations in (36) and property (76), it can be concluded that the largest invariant set is, in the worse case, when $K_{p\vartheta}\, sinh\left(2\, \ln \boldsymbol{q}_e\right) = \vec{\zeta}_{\vartheta_e}$, which only occurs at the origin by the fact that $\|K_{p\vartheta}\| > 2\, L_{\vec{\zeta}_{\Omega_e}}$ (see following analysis). Therefore, the attitude system in (36) is asymptotically stable. R1Q3

Analysis of condition (39)

Substituting (73) into (39), it follows that R1Q3

$$\begin{aligned} \frac{\partial g\left(\boldsymbol{q}_e, \vec{\Omega}_e\right)}{\partial \vec{\Omega}_e} J^{-1} \left[K_{d\vartheta} \vec{\Omega}_e + K_{p\vartheta} sinh\left(2 \ln \boldsymbol{q}_e\right)\right] \geq & \left[\left\|\frac{\partial g\left(\boldsymbol{q}_e, \vec{\Omega}_e\right)}{\partial \vec{\Omega}_e}\right\| \left\|J^{-1}\right\| L_{\vec{\zeta}_{\Omega_e}} + \right. \\ & \left. \frac{1}{2} \left\|\frac{\partial g\left(\boldsymbol{q}_e, \vec{\Omega}_e\right)}{\partial \boldsymbol{q}_e}\right\|\right] \left\|\vec{\Omega}_e\right\| \\ & + \left[\left\|\frac{\partial g\left(\boldsymbol{q}_e, \vec{\Omega}_e\right)}{\partial \vec{\Omega}_e}\right\| \left\|J^{-1}\right\| L_{\vec{\zeta}_{\Omega_e}} + \right. \\ & \left. \left\|\sum_i f_i\right\| \left\|\frac{\partial f\left(\dot{\vec{p}}_e, \vec{p}_e\right)}{\partial \vec{p}_e}\right\|\right] \left\|2 \ln \boldsymbol{q}_e\right\| \\ \Longrightarrow \quad \vec{\Omega}_e^T \left[K_{d\vartheta} \vec{\Omega}_e + K_{p\vartheta} sinh\left(2 \ln \boldsymbol{q}_e\right)\right] \geq & \left[\left\|\vec{\Omega}_e\right\| L_{\vec{\zeta}_{\Omega_e}} + \right. \\ & \left. \frac{1}{2} \left(K_{p\vartheta} sinh\left(2 \ln \boldsymbol{q}_e\right) - \vec{\zeta}_{\vartheta_e}\right)\right] \left\|\vec{\Omega}_e\right\| \\ & + \left(\left\|\vec{\Omega}_e\right\| L_{\vec{\zeta}_{\Omega_e}} + \left\|\dot{\vec{p}}_e\right\| \right. \\ & \left. \left\|m\vec{g} - K_{dt}\dot{\vec{p}}_e - \right. \right. \\ & \left. \left. K_{pt} \tanh \vec{p}_e\right\|\right) \left\|2 \ln \boldsymbol{q}_e\right\| \end{aligned} \tag{78}$$

The terms depending on $\|2\,\ln \boldsymbol{q}_e\|$ are grouped in the following inequality R1Q3

$$\begin{aligned} \tfrac{1}{2}\left\|\vec{\Omega}_e\right\| \|K_{p\vartheta}\| \|sinh\,(2\ln \boldsymbol{q}_e)\| \geq & \left(\tfrac{1}{2}\left\|\vec{\Omega}_e\right\| L_{\vec{\zeta}_{\Omega_e}} + \left\|\dot{\vec{p}}_e\right\| \|m\vec{g} - \right. \\ & \left. K_{dt}\dot{\vec{p}}_e - K_{pt}\tanh \vec{p}_e\right\|\Big) \|2\ln \boldsymbol{q}_e\| \\ \geq & \left[\tfrac{1}{2}\left\|\vec{\Omega}_e\right\| L_{\vec{\zeta}_{\Omega_e}} + \left\|\dot{\vec{p}}_e\right\| \left(\|m\vec{g}\| + \left\|K_{dt}\dot{\vec{p}}_e\right\| + \right.\right. \\ & \left.\left. \|K_{pt}\|\right)\right] \|2\ln \boldsymbol{q}_e\| \\ \Longrightarrow \quad \|K_{p\vartheta}\| \|sinh\,(2\ln \boldsymbol{q}_e)\| \geq & \left[L_{\vec{\zeta}_{\Omega_e}} + \frac{2\|\dot{\vec{p}}_e\|\left(\|m\vec{g}\| + \left\|K_{dt}\dot{\vec{p}}_e\right\| + \|K_{pt}\|\right)}{\left\|\vec{\Omega}_e\right\|}\right] \|2\ln \boldsymbol{q}_e\| \end{aligned} \tag{79}$$

The effect produced by the coupled dynamics on the stability of the system is presented in the following term

$$\epsilon_\vartheta := \frac{2\left\|\dot{\vec{p}}_e\right\|\left(\|m\,\vec{g}\| + \left\|K_{dt}\,\dot{\vec{p}}_e\right\| + \|K_{pt}\|\right)\|2\,\ln \boldsymbol{q}_e\|}{\left\|\vec{\Omega}_e\right\|} \tag{80}$$

A key difference between this term and the one presented in (61) is that, as the translation control law (68) is bounded in the position dynamics because of the term $-K_{pt}\,\tanh \vec{p}_e$, ϵ_ϑ has a constant effect that does not depend explicitly on the state variable $\vec{p}_e$. Substituting (80) into (79) results in R1Q3

$$\|K_{p\vartheta}\|\,\|sinh\,(2\,\ln \boldsymbol{q}_e)\| \geq \quad L_{\vec{\zeta}_{\Omega_e}}\,\|2\,\ln \boldsymbol{q}_e\| + \epsilon_\vartheta \tag{81}$$

If only small translation velocities are considered, then $\epsilon_\vartheta \approx 0$, which implies that if $\|K_{p\vartheta}\| > 2\,L_{\vec{\zeta}_{\Omega_e}}$ is enforced, the condition is met for these terms.

The terms that depend solely on $\left\|\vec{\Omega}_e\right\|$ can be grouped as

$$\begin{aligned} \left\|\vec{\Omega}_e\right\|^2 \|K_{d\vartheta}\| \geq & \left\|\vec{\Omega}_e\right\|^2 L_{\vec{\zeta}_{\Omega_e}} \\ \Longrightarrow \qquad \|K_{d\vartheta}\| \geq & L_{\vec{\zeta}_{\Omega_e}} \end{aligned} \tag{82}$$

where $K_{d\vartheta}$ is chosen in order to enforce the previous inequality, which results in system (5) - (6) being asymptotically stable with control inputs (68) and (73).

4.3. Separated saturations control law

A more thorough description for this type of controller can be found in Castillo et al. (2004). The advantage of a control law based on separated saturations is that it takes into consideration the inherent nature that most actuators have a bounded operation limit. This type of nonlinear behavior is problematic in control strategies that assume an unbounded operation limit. The main objective of the proposed controller is to bound the total effect of the position control law in order for the attitude controller to better reach the orientation reference.

Let us start by defining the saturation function $\varsigma_\beta\,(\cdot) : \mathbb{R}^n \to \mathbb{R}^n$ for a vector $\vec{a} \in \mathbb{R}^n$ and a positive constant scalar $\beta \in \mathbb{R}_+$ as R1Q3

$$\varsigma_{\beta}\left(\vec{a}\right) \coloneqq \begin{cases} \vec{a} & , \|\vec{a}\| < \beta \\ \beta\, sgn\left(\vec{a}\right) & , \|\vec{a}\| \geq \beta \end{cases} \tag{83}$$

where the **sign** function $sgn\left(\cdot\right) : \mathbb{R}^n \to \mathbb{R}^n$ is defined element-wise.

Propose the following controllers based on saturation functions,

$$\begin{aligned} \vec{F}_u = &\; m\,\vec{g} - K_{dt}\,\varsigma_{\beta_d}\left(\dot{\vec{p}}_e\right) - K_{pt}\,\varsigma_{\beta_p}\left(K_{dt}\,\vec{p}_e + \dot{\vec{p}}_e\right) \\ \vec{\tau} = &\; \vec{\Omega} \times J\,\vec{\Omega} - K_{d\vartheta}\,\vec{\Omega}_e - K_{p\vartheta}\left(2\,\ln \boldsymbol{q}_e\right) \end{aligned} \tag{84}$$

where $K_{pt}, K_{dt}, K_{p\vartheta}, K_{d\vartheta} \in \mathbb{R}^{3\times 3}_{+}$ are constant gain matrices such that $K_{p\vartheta} > 2\,L_{\vec{\zeta}_{\Omega_e}}$, $K_{d\vartheta} > L_{\vec{\zeta}_{\Omega_e}}$, $\|K_{dt}\| > L_p$.

The perturbation into the translation system is assumed to be very small and absorbed into the effects of the term $\vec{\zeta}_{\Omega_e}$. Using the function V_{q_e} given in (49), propose the following Lyapunov candidate function for the translation system

$$V_{p_e} = \frac{\dot{\vec{p}}_e^{\,T}\,\dot{\vec{p}}_e}{2} + \frac{\left(\dot{\vec{p}}_e + K_{dt}\,\vec{p}_e\right)^T\left(\dot{\vec{p}}_e + K_{dt}\,\vec{p}_e\right)}{2} \tag{85}$$

Differentiating V_{p_e}, w.r.t. time results in

$$\begin{aligned} \dot{V}_{p_e} = &\; \dot{\vec{p}}_e^{\,T}\left[-K_{dt}\,\varsigma_{\beta_d}\left(\dot{\vec{p}}_e\right) - K_{pt}\,\varsigma_{\beta_p}\left(\dot{\vec{p}}_e + \right.\right. \\ &\left.\left. K_{dt}\,\vec{p}_e\right)\right] + \left(\dot{\vec{p}}_e + K_{dt}\,\vec{p}_e\right)^T\left[-K_{pt}\,\varsigma_{\beta_p}\left(\dot{\vec{p}}_e + K_{dt}\,\vec{p}_e\right)\right] \\ = &\; -\dot{\vec{p}}_e^{\,T} K_{pt}\,\varsigma_{\beta_p}\left(\dot{\vec{p}}_e\right) - \left(\dot{\vec{p}}_e + \dot{\vec{p}}_e + K_{dt}\,\vec{p}_e\right)^T K_{pt}\,\varsigma_{\beta_p}\left(\dot{\vec{p}}_e + K_{dt}\,\vec{p}_e\right) \end{aligned} \tag{86}$$

where the term $-\dot{\vec{p}}_e^{\,T}\,K_{pt}\,\varsigma_{\beta_p}\left(\dot{\vec{p}}_e + K_{dt}\,\vec{p}_e\right)$ was factored from the first term to the second. Taking into account the inequality $\left\|\dot{\vec{p}}_e\right\| \leq \left\|\dot{\vec{p}}_e + K_{dt}\,\vec{p}_e\right\|$, $\dot{V}_{p_e}$ can be further simplified

$$\dot{V}_{p_e} \leq \; -\dot{\vec{p}}_e^{\,T} K_{pt}\,\varsigma_{\beta_p}\left(\dot{\vec{p}}_e\right) - \left(\dot{\vec{p}}_e + K_{dt}\,\vec{p}_e\right)^T K_{pt}\,\varsigma_{\beta_p}\left(\dot{\vec{p}}_e + K_{dt}\,\vec{p}_e\right) \leq 0 \tag{87}$$

Similarly for the rotational dynamics, differentiating V_{q_e} given in (49), w.r.t. time results in the equation (58). Therefore, the controllers presented in (84) stabilize system (36).

Analysis of condition (39)

Following the design scheme in Theorem 3.4, the inequality (39) will be analyzed for the proposed control laws in order to determine asymptotic stability.

Substituting (84) into (39) results in

$$\begin{aligned} -\|P_\Omega\|\left\|\vec{\Omega}_e\right\|\left(\|K_{p\vartheta}\|\,\|2\ln \boldsymbol{q}_e\| + \|K_{d\vartheta}\|\left\|\vec{\Omega}_e\right\|\right) \leq &\; -\left[\|P_\Omega\|\left\|\vec{\Omega}_e\right\|\left\|J^{-1}\right\| L_{\vec{\zeta}_{\Omega_e}} + \right. \\ &\left. \|P_p\|\left\|\dot{\vec{p}}_e\right\|\left\|\sum_i f_i\right\|\right]\|2\ln \boldsymbol{q}_e\| \\ &-\left[\|P_\Omega\|\left\|\vec{\Omega}_e\right\|\left\|J^{-1}\right\| L_{\vec{\zeta}_{\Omega_e}} + \right. \\ &\left. \frac{1}{2}\|P_\Omega\|\,\|2\ln \boldsymbol{q}_e\|\right]\left\|\vec{\Omega}_e\right\| \end{aligned} \tag{88}$$

The terms depending on $\|2\ \ln \boldsymbol{q}_e\|$ are grouped in the following inequality

$$\begin{aligned} -\|P_\Omega\| \left\|\vec{\Omega}_e\right\| \|K_{p\vartheta}\| \|2\ \ln \boldsymbol{q}_e\| \leq & -\left(\left\|J^{-1}\right\| L_{\vec{\zeta}_{\Omega_e}} + \tfrac{1}{2}\right) \|P_\Omega\| \left\|\vec{\Omega}_e\right\| \|2\ \ln \boldsymbol{q}_e\| \\ & - \|P_p\| \left\|\dot{\vec{p}}_e\right\| \left\|\sum_i f_i\right\| \|2\ \ln \boldsymbol{q}_e\| \\ \implies -\|P_\Omega\| \left\|\vec{\Omega}_e\right\| \|K_{p\vartheta}\| \leq & -\left(\left\|J^{-1}\right\| L_{\vec{\zeta}_{\Omega_e}} + \tfrac{1}{2}\right) \|P_\Omega\| \left\|\vec{\Omega}_e\right\| - \|P_p\| \left\|\dot{\vec{p}}_e\right\| \left\|\sum_i f_i\right\| \\ \implies \|K_{p\vartheta}\| \geq & \left\|J^{-1}\right\| L_{\vec{\zeta}_{\Omega_e}} + \tfrac{1}{2} + \frac{\|P_p\| \left\|\dot{\vec{p}}_e\right\| \left\|\sum_i f_i\right\|}{\|P_\Omega\| \left\|\vec{\Omega}_e\right\|} \end{aligned} \tag{89}$$

In this case, the effect produced by the coupled dynamics on the stability of the system is mainly presented in the last term of (89), which can be defined as

$$\epsilon_\vartheta := \frac{\|P_p\| \left\|\dot{\vec{p}}_e\right\| \left\|\sum_i f_i\right\|}{\|P_\Omega\| \left\|\vec{\Omega}_e\right\|} \tag{90}$$

and depends on the vehicle's saturated thrust force $\left\|\sum_i f_i\right\|$ and the velocity dynamics, which also tends to be saturated if the effect of the translation controller is successfully applied to the system.

Substituting ϵ_ϑ into (89) yields

$$\|K_{p\vartheta}\| \geq \left\|J^{-1}\right\| L_{\vec{\zeta}_{\Omega_e}} + \frac{1}{2} + \epsilon_\vartheta \tag{91}$$

Observe that, if $\|P_\Omega\| >> \|P_p\|$, then $\epsilon_\vartheta \approx 0$, which makes its effect negligible. A key difference with the state-feedback controller presented before is that this condition is less restrictive because the terms $\left\|\sum_i f_i\right\|$ and $\left\|\dot{\vec{p}}_e\right\|$ are bounded due to the nature of the separated saturations control scheme. Therefore, the condition is met if $K_{p\vartheta}$ is chosen such that (91) is enforced.

The terms from (88) that depend solely on $\left\|\vec{\Omega}_e\right\|$ can be grouped as

$$\begin{aligned} -\|P_\Omega\| \left\|\vec{\Omega}_e\right\|^2 \|K_{d\vartheta}\| \leq & -\|P_\Omega\| \left\|\vec{\Omega}_e\right\|^2 \left\|J^{-1}\right\| L_{\vec{\zeta}_{\Omega_e}} \\ \implies \|K_{d\vartheta}\| \geq & \left\|J^{-1}\right\| L_{\vec{\zeta}_{\Omega_e}} \end{aligned} \tag{92}$$

If $K_{d\vartheta}$ is chosen in order to enforce (92), it can be concluded that system (5) - (6) is asymptotically stable to the equilibrium point (40) with control inputs (84).

5. Results

The proposed control approach has been validated with numeric simulations and experimental results. This corroborates its effectiveness to stabilize the family of under actuated systems using different control schemes.

5.1. Simulations

The simulations are made using two different scenarios (A and B) that are designed to test the agility and robustness of the proposed controllers. The general physical parameters of the vehicle are shown on Table 1.

R1Q4

J	g	m
$\text{diag}\left(\begin{bmatrix}0.006 & 0.006 & 0.4\end{bmatrix}\left[kg\,m^2\right]\right)$	$9.81\left[\frac{m}{s^2}\right]$	$1.2\,[kg]$

Table 1.: Physical parameters used for the numerical simulations.

Scenario A In this scenario, the aerial vehicle must follow a circular trajectory with a constant radius (2 $[m]$), height (2 $[m]$) and speed (2 $[m/s]$). In this case, the free DOF of the vehicle is used to force the front of the quadcopter to always look at the inside of the circle in order to completely test the attitude controllers. In order to be able to stay within the circle, the platform needs to exert an almost constant force pointing at the center of the circle. The desired speed is directly proportional to the magnitude of this force, and forces the quadcopter to have an inclination w.r.t. the ground level.

We have simulated the performance of the three proposed controllers, for paper length restrictions, we include here the performance of the Separated Saturations Controller (SSC) (84). Nevertheless, the results of the other control laws (51) and (68) can be found in the supplementary material. Editor

Observe in Figure 4 the good performance of the system when following the circular trajectory. Notice also from Figures 4 and 5 that the imposed constraints are satisfied.

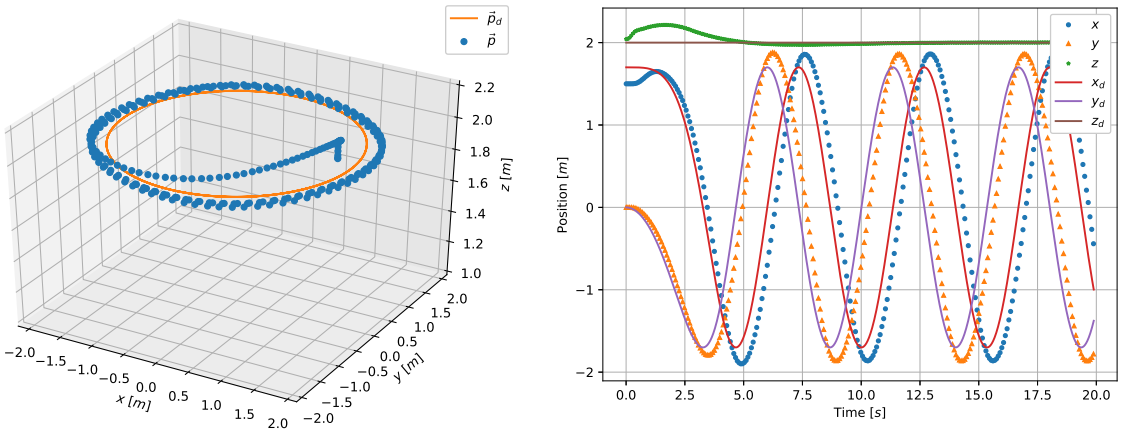

(a) 3D path when using the SSC algorithm.

(b) Translational reference tracking

Figure 4.: Simulation results for scenario A when using the SSC. The position of the vehicle is depicted using markers of different kinds, and the desired trajectory is shown using solid lines.

The virtual control, which is the desired force obtained by the position control part of the algorithm, is illustrated for the SSC in Figure 6. The force in the z axis is located near a constant value because it is opposing the gravity's effect on the system. Figure 7 illustrates the real thrust force and torques of the system. The real thrust force is computed from the virtual control inputs.

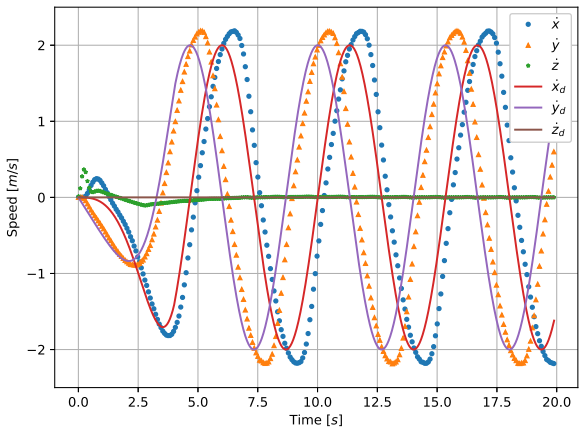

Figure 5.: Speed plot of the vehicle for scenario A.

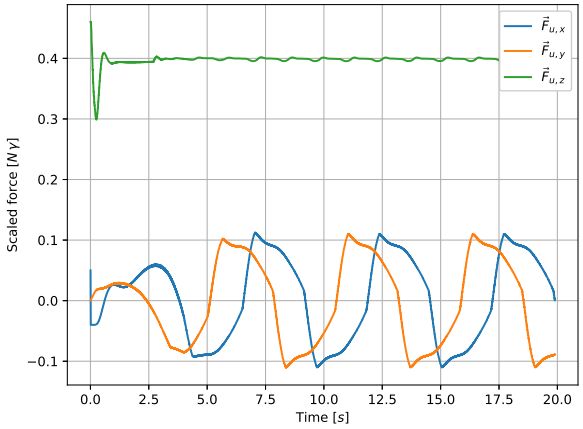

Figure 6.: Control inputs performance of the controller SSC. The force is scaled because of the parameters of the motors.

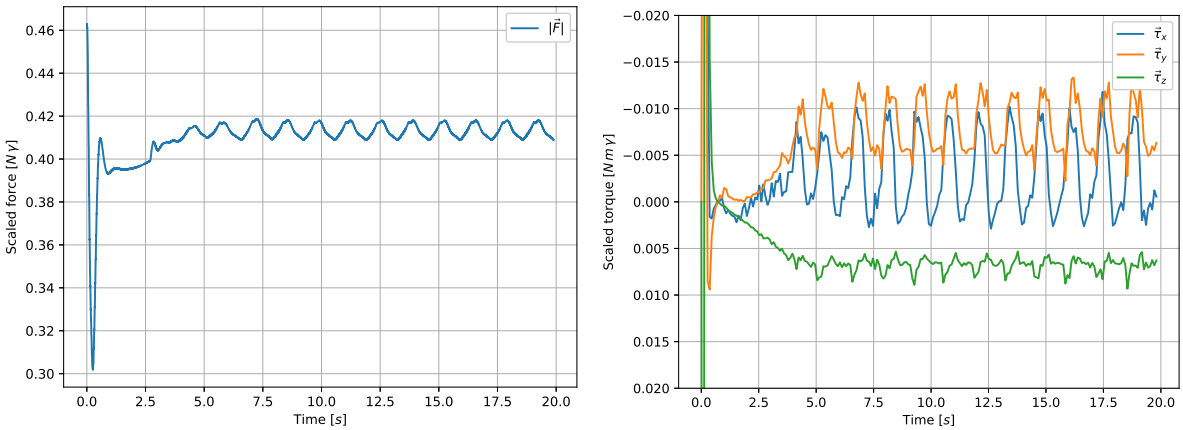

(a) Real-thrust force performance.

(b) Torque behaviors.

Figure 7.: Real-time performances of the real control inputs in the system for scenario A and when using the SSC algorithm. The thrust and the torques are both scaled.

Figure 8 depicts the rotational subsystem behavior. The left figure illustrates how the quaternion reference (computed from control inputs using (13) and (14)) is tracked by the controller

(84). The equivalent Euler angles representation is shown in the right column for illustration purposes. Notice in Figure 8b that the pitch and roll angle are changing from 7 ° for keeping the imposed velocity constraint.

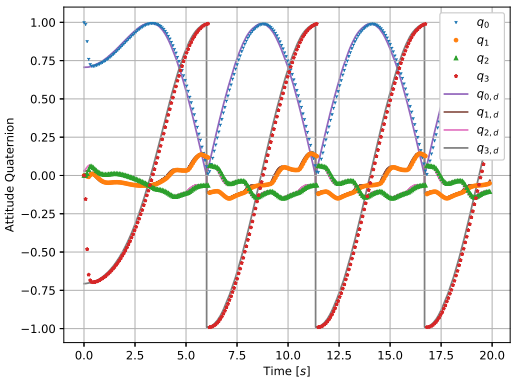

(a) Quaternion reference tracking when using the SSC algorithm.

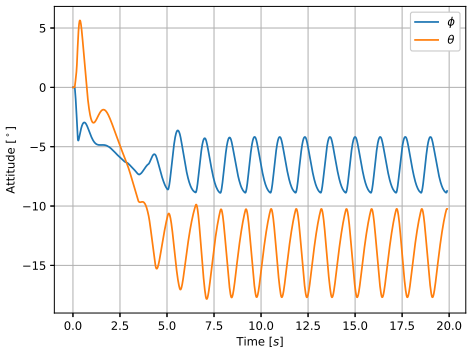

(b) Euler angles roll ϕ and pitch θ equivalent representation of the attitude tracking performance using SSC.

Figure 8.: Quadcopter attitude simulation for scenario A using the separated saturations controller (84).

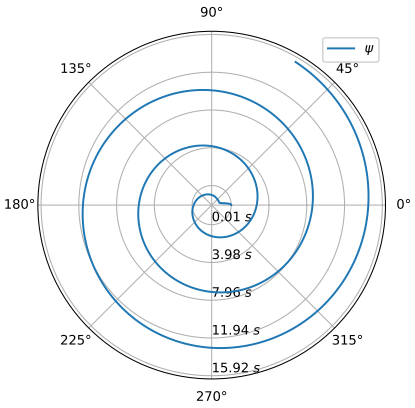

Figure 9.: Quadcopter yaw ψ attitude for the simulation of scenario A using the separated saturations controller (84). The angle is shown using a polar plot in order to showcase the circle maneuver. The radius of the plot represents time in seconds.

Scenario B In this scenario, we propose a quick change of reference into the system with constant acceleration to observe the quadcopter's reaction. The goal here is to analyze the reactivity of the drone when it needs to flee suddenly from an incoming danger. The trajectory is described in two movements : the first one is a constant acceleration reference in one axis and the parameters used are the distance ($2\,[m]$) to advance, and the desired time ($0.7\,[s]$) to reach it. The second movement is a constant position reference for a fixed waiting time of $3\,[s]$, before returning to the original position and repeating. Again, we have validated this scenario for the three proposed controllers. In this case, we have choose to present the performance of the system when using the state feedback controller (51). The other graphs from the other controllers can be located in the supplementary material. R1Q4 Editor

Observe from Figure 10a that the altitude for the vehicle tends to remain constant throughout the maneuver. Most controllers in these types of scenarios for the quadcopter platform tend to sacrifice the altitude for a gain in speed. Because of how our proposed strategy successfully

separates the translational from the attitude dynamics, the changes in the altitude dynamics can be considered negligible. Notice also from Figure 10b that the virtual control input for the x axis remains close to zero, while for the y axis is changing. It is due to fact that the only movement of the aerial vehicle is in the y axis.

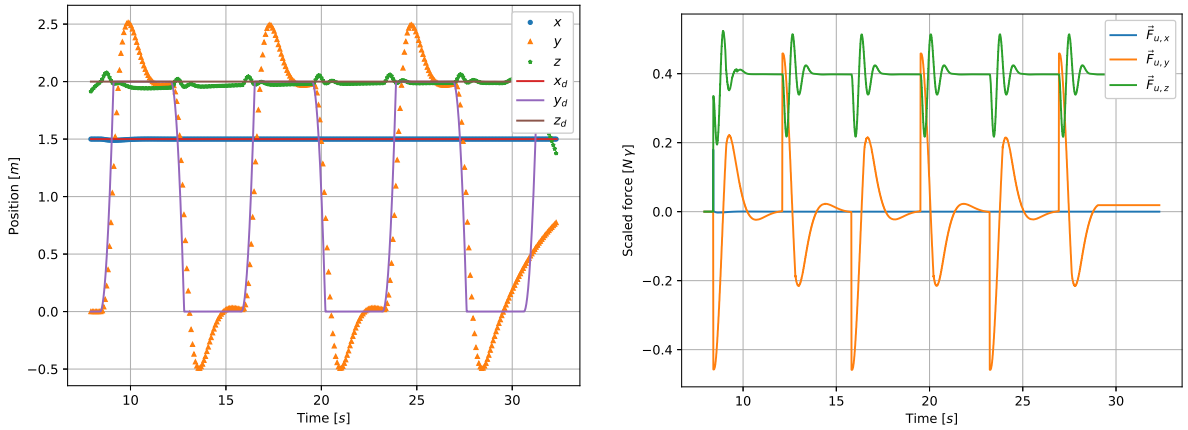

(a) The position of the vehicle using the SFC. The reference trajectory is only applied on the y axis.

(b) The virtual control inputs for the SFC.

Figure 10.: Position performance of the system and virtual control inputs from simulation using Scenario B and the SFC algorithm.

In Figure 11 the real thrust force and torques applied into the system are illustrated. Notice from the zoom in Figure 11b that the only parameter that is changing is the torque for the y axis and the others remain close to zero.

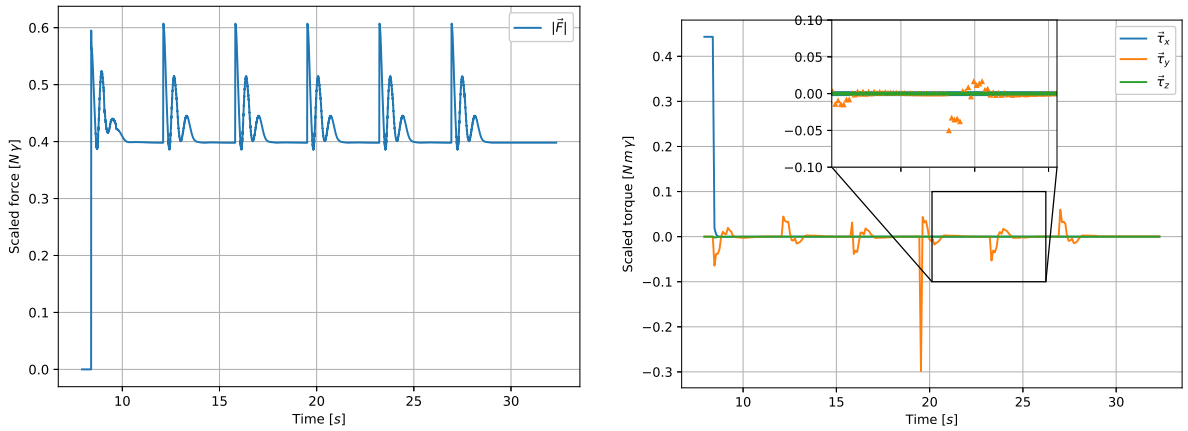

(a) The thrust force used by the SFC

(b) The torques used by the SFC

Figure 11.: Simulation results for scenario B when using the SFC. The thrust and the torques are both scaled.

The attitude performance and its corresponding reference for this scenario when the controller (51) is applied can be seen in Figure 12. The orientation control is able to closely follow the changes in the reference of the position controller. Notice also in Figure 12b the Euler angle representation of this attitude performance. In this figure it can be appreciated that the aerial vehicle reaches aggressive pitch angles of $|60°|$.

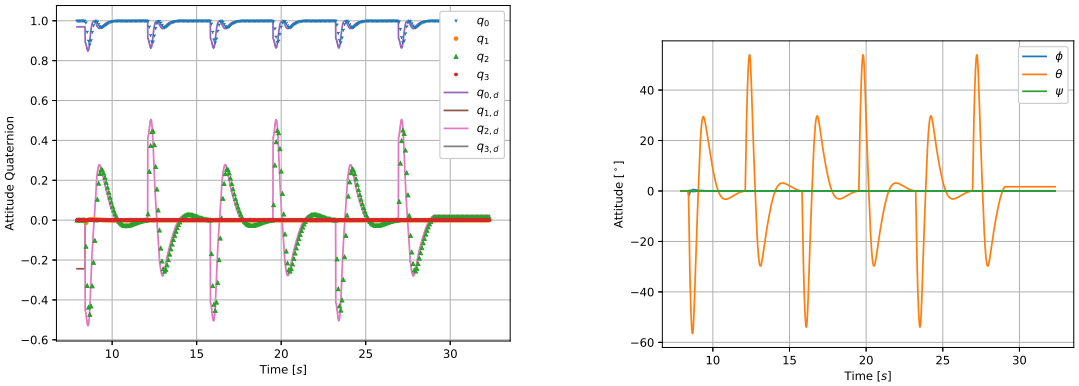

(a) Quaternion reference tracking when using (51). (b) Euler angles equivalent representation of the attitude tracking performance.

Figure 12.: Quadcopter attitude simulation for scenario B when using the controller (51).

5.2. Experimental results

Three experiments were performed on an AR-Drone 2.0 commercial UAV, the factory firmware was substituted by the one included in our FLAIR framework, see Sanahuja (2016). For validating our control proposition, the translational information (position and velocity) were estimated by a motion capture system, while the rotational states were obtained from the drone's inertial measurement unit. For real-life scenarios, a GPS RTK sensor can be used for measuring/estimating the position of the aerial vehicle and for improving measurement or completing the remained states an observer (as Kalman Filter) can be used.

In our experiments, the embedded system runs in soft real-time and the sampling period is on average 5.516212206539637 $[ms]$, with a minimum delay of 2.1970272064208984 $[ms]$ and a maximum delay of 7.708466053009033 $[s]$. Notice that even under these circumstances with delays, the strategy was robust enough to yield successful results in all scenarios. R1Q4

The flight-tests scenarios are the same ones used in simulations, nevertheless, an additional scenario (C) is proposed to showcase the robustness of the strategy against external conditions. *Scenario C* consists on giving the vehicle a constant position reference and use an external wind blower machine to try to destabilize the system.

Scenario A In this scenario (tracking a circular trajectory), the parameters for the flight tests are ; circle trajectory radius 1.5 $[m]$, altitude 1.2$[m]$ and velocity $\approx$ 2.5 $[m/s]$. In the following figures, the system performances are illustrated when using the controller SSC. The other control performances for this scenario are presented in the supplementary material . A video illustrating these results can be accessed at *https://youtu.be/PaHk3fyeShc* R1Q4 Editor

Notice from Figure 13 the well performance of the system when using the control algorithm (84). Observe from Figure 13b that all the states converge to the desired values for tracking the trajectory. In addition, the performance presented in Figure 13 shows a stable position tracking error. This can indicate how robust control algorithms can be obtained for a quadcopter platform using the proposed design methodology even in real-world scenarios. Notice from Figure 14 that the desired velocities imposed in the vehicle are well tracked.

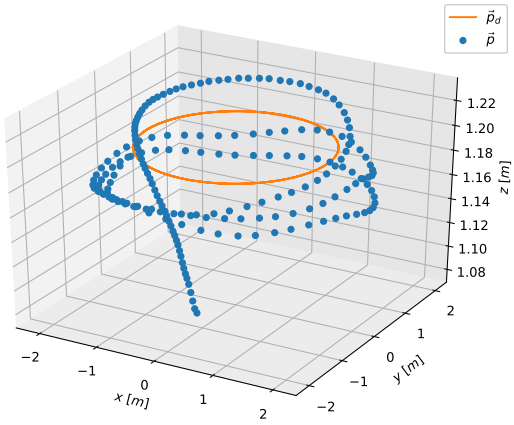

(a) 3D system performance when tracking a circular trajectory.

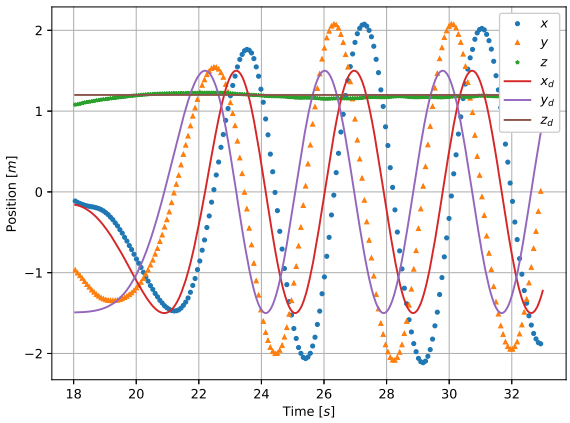

(b) Real-time position behavior of the system.

Figure 13.: System real-time performance for scenario A and using the SSC algorithm.

.

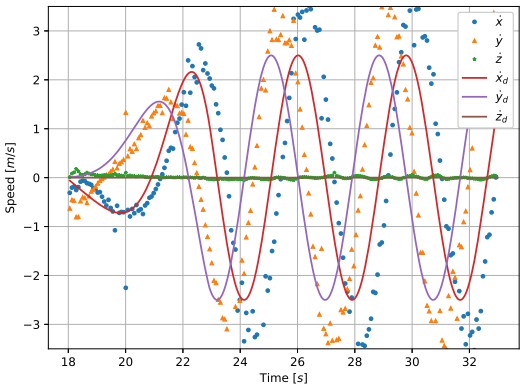

Figure 14.: Speed plot of the vehicle for Scenario A in real-time experiments.

The virtual and the real control inputs for this controller (SSC) are depicted in Figures 15 and 16. Notice from these figures a similar performance obtained from simulations.

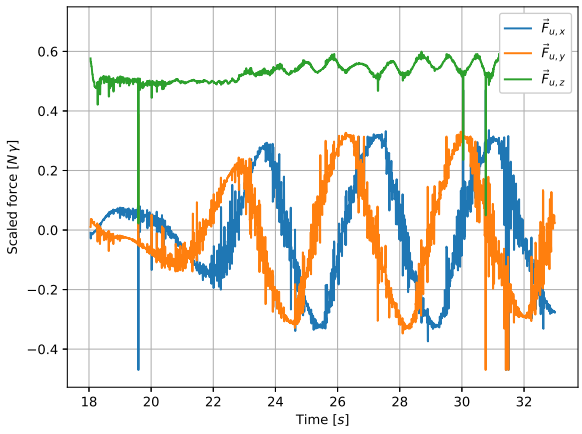

Figure 15.: Virtual control inputs performances.

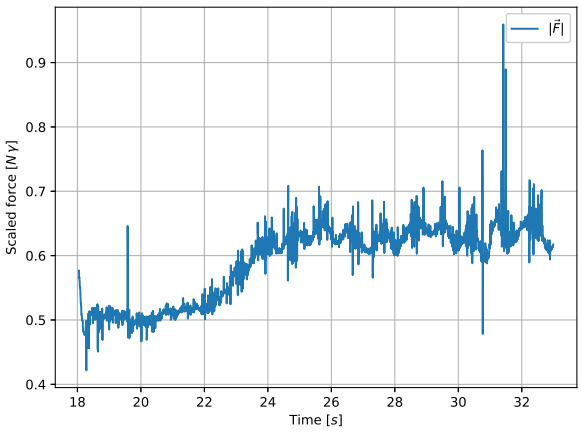

(a) The thrust force used by the SSC

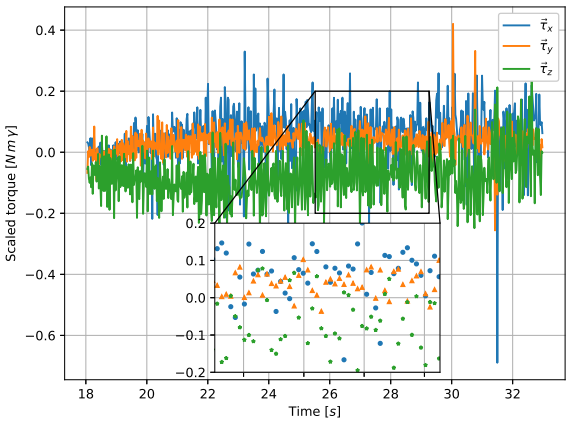

(b) The torques used by the SSC

Figure 16.: Real control input behavior for scenario B when using the SSC. The thrust and the torques are both scaled.

Figure 17 illustrates the rotational subsystem behavior. Observer in Figure 17a the attitude quaternion performance of the system. This figure is difficult to analyze, nevertheless, we added in Figure 17b its corresponding Euler angle representation. The discontinuities that occur both in the reference and the attitude of the quadcopter in Figure 17a is a consequence of enforcing the restriction $q_0 \geq 0$ in order to compensate for the unwinding effect of the quaternion representation. Even though this restriction makes it seem like the movements are discontinuous, this is not the case.

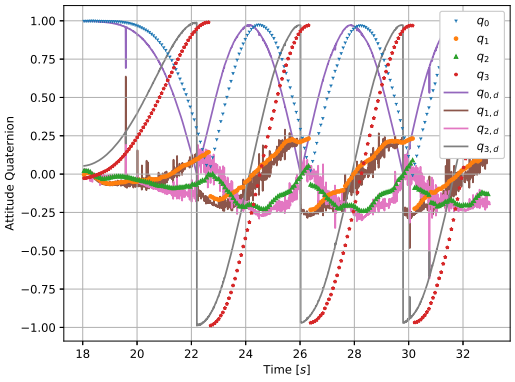

(a) Attitude quaternion performance.

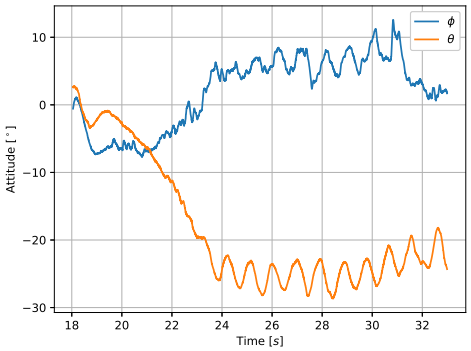

(b) Euler angles equivalent representation of the attitude tracking performance.

Figure 17.: Quadcopter attitude real-time performance for Scenario A when using the separated saturations controller.

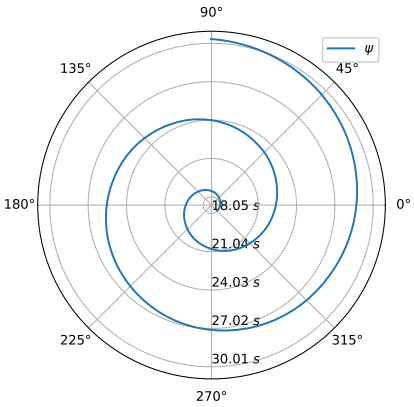

Figure 18.: Quadcopter yaw ψ attitude for the experiments of scenario A using the separated saturations controller (84). The angle is shown using a polar plot in order to showcase the circle maneuver. The radius of the plot represents time in seconds.

Scenario B In this scenario (sudden changes of references with constant acceleration), the parameters for the flight tests are; time used for the translation 0.8 $[s]$, resting time 5 $[s]$, and desired altitude of 1.2$[m]$. In the following we introduce the results when applying the controller SSC (84). The performances of the other controllers can be seen in the supplementary material. A demonstration video of this case is available at *https://youtu.be/8G9s12AloP8* R1Q4 Editor

From 19a observe the well performance of the system for tracking the reference in the y axis, notice also that the altitude remains close to the desired value and the x position is close to zero. Similarly, from Figure 19b observe that the virtual force for the y axis is changing for moving the vehicle to the desired values. The virtual force in the z axis also changes for keeping the desired altitude. The performance of the real control inputs in the system can be seen in Figure 20.

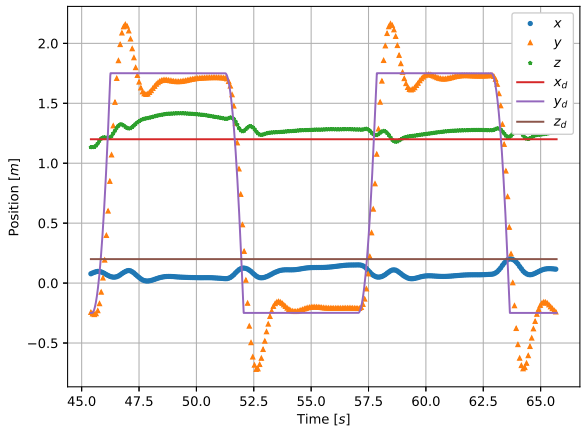

(a) The position of the vehicle using the SSC. The reference trajectory is only applied on the y axis.

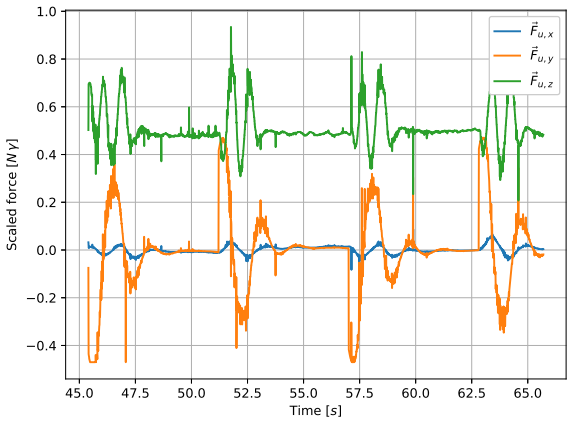

(b) The virtual control inputs for the SSC.

Figure 19.: Position results and virtual control inputs for the experiments using Scenario B and the SSC.

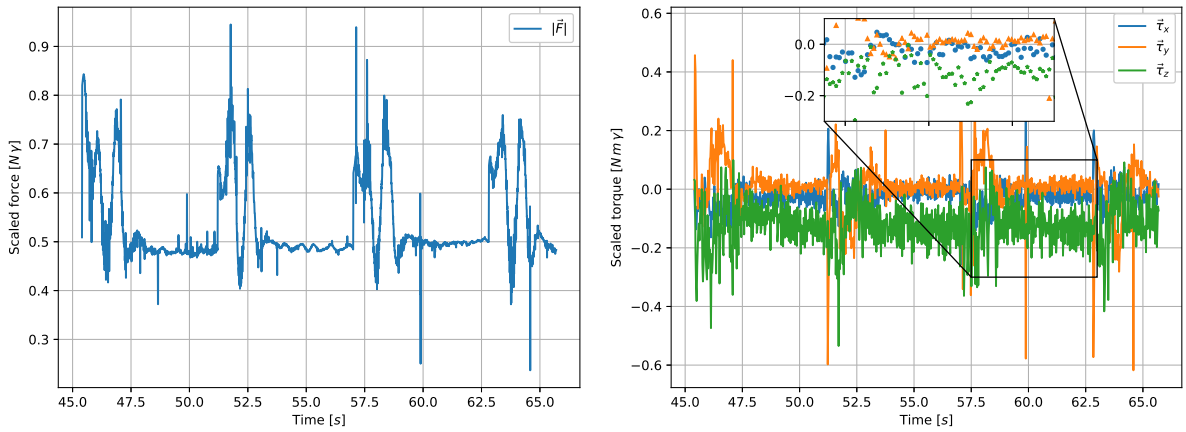

(a) The thrust force used by the SSC

(b) The torques used by the SSC

Figure 20.: Real control input performances obtained in scenario B when using the SSC. The thrust and the torques are both scaled.

The attitude performance and its reference for experimental tests in Scenario B using the SSC can be seen in Figure 21. The orientation control is able to closely follow the changes in the reference of the position controller as showed in Figure 19a. Notice from Figure 21b that the pitch angle reaches aggressive values of $|45°|$.

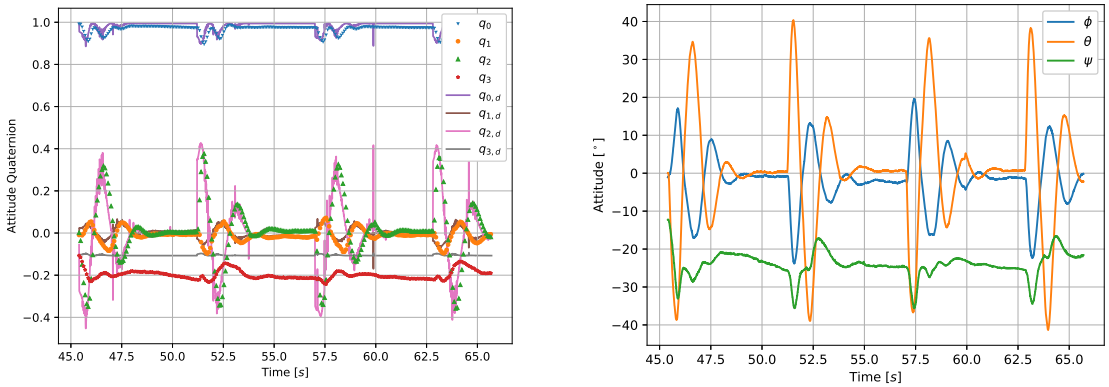

(a) Quaternion reference tracking using the SSC

(b) Euler angles equivalent representation of the attitude tracking performance using SSC.

Figure 21.: Quadcopter attitude performances obtained from real-time experiments for Scenario B and using the separated saturations controller (84).

Scenario C: In this scenario the goal is that the quadcopter remains at hover and closes to its desired position while it is exposed to strong external and unknown disturbances. This scenario is used to verify that the proposed method generates controllers that are robust against external perturbations. These external disturbances were produced using a wind blower capable of generating winds at $60\,[km/h]$ and it was placed between 1 $[m]$ and 1.5 $[m]$ from the drone. The parameters for the flight tests are : $z_d = 1.5$ $[m]$, $x_d = 0.05$ $[m]$ and $y_d = 0.2$ $[m]$. In the following graphs the experimental results when the controller SFC (51) is applied into the system. The other performances of the other two controllers are presented in the supplementary material. A video exposing these experiments is available at *https://youtu.be/7D2BKoUSF-I* R1Q4 Editor

In Figure 22a the position performances of the system when applied the controller for this scenario are presented. In Figure 22b their respective virtual control inputs. Observe from Figure 23 the real thrust force and torques applied to the aerial platform.

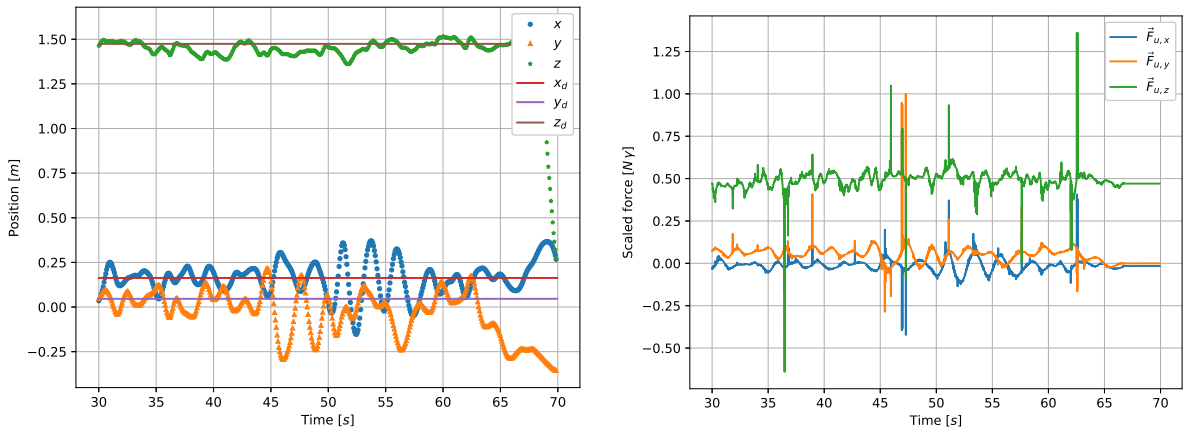

(a) Position performances of the system when it is exposed to wind gust.

(b) Virtual control behaviors for achieving the desired mission.

Figure 22.: Position results and virtual control inputs for the real-time experiments using Scenario C and the control law (51).

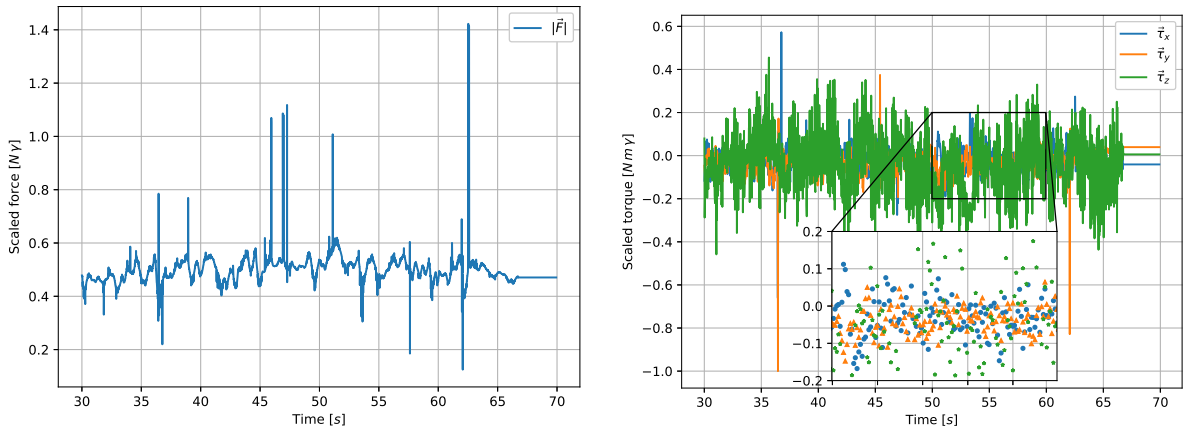

(a) Thrust force performance obtained from the virtual control inputs.

(b) Control torques applied to the aerial platform.

Figure 23.: Real control input performances obtained in scenario B when using the SFC. The thrust and the torques are both scaled.

The attitude behavior with respect to their references for this scenario C can be seen in Figure 24. Observe that the orientation control torques (in Figure 11b) are able to keep the system closely to the desired position even in presence of external disturbances. For better appreciate this performance its corresponding Euler angle representation is given in Figure 24b. Notice from Figure 22a that our controller is robust with respect to unknown and external disturbances. For improving system's performances other solutions, as well as robust controllers, are to use observers for estimating the perturbations and include them into the closed-loop system.

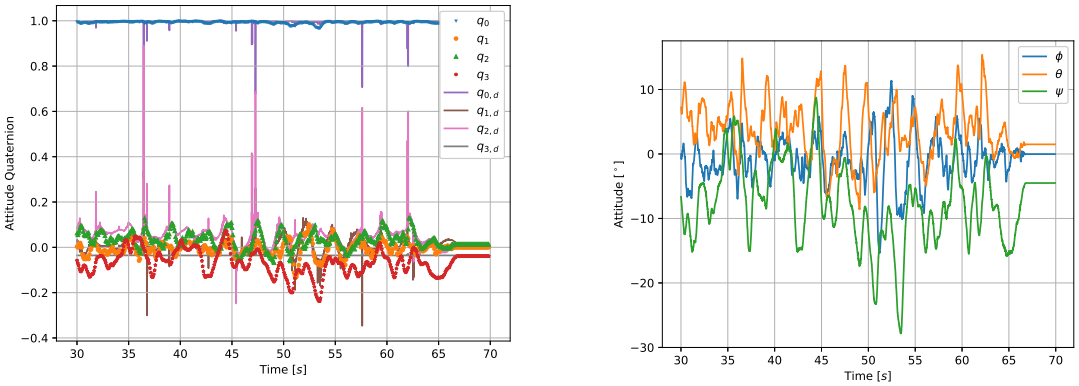

(a) Quaternion attitude performances.

(b) Euler angles equivalent representation of the attitude tracking performance.

Figure 24.: Quadcopter attitude performance obtained in Scenario C and using the state feedback controller. Notice that the inclination required to compensate the disturbances is robustly managed by the controller.

6. Conclusions and Discussions

A method to control a family of under actuated systems was designed, validated, simulated and tested in this work. The main characteristic of this family of systems is that the direction of the actuator's translation forces, the ones that change the position of the vehicle, directly depends on the attitude state of the system. Many vehicle platforms can be included in this category, like multicopter platforms, underwater vehicles, fixed-winged aircraft, to name a few.

The design strategy started with a viable controller for an equivalent fully actuated rigid-body dynamic model. This control law must consist of two independent control algorithms, one for the position dynamics and one for the attitude system, and they both need to have associated with them a Lyapunov candidate function that guarantees stability for the fully actuated system. The orientation dynamics are represented using quaternions. These controllers must also satisfy condition (39).

Once a suitable pair of control laws has been selected, the attitude control can be adapted to the original under actuated system by means of an internal quaternion reference trajectory, defined in equation (15). Section 3 delves deeper into the mathematical basis and construction of this reference trajectory. In comparison with other reference trajectories, it can be shown that the one proposed is optimal in the sense that it indicates the shortest rotation that the system must do in order to align the desired thrust force with the real one, as shown in Lemma 2. This in itself gives the proposed method an edge over others methodologies that use Euler angles. The design and implementation of the proposed control strategy for the under actuated system was presented in Theorem 3.4.

In order to corroborate the presented strategy, three example cases with different control paradigms were designed with the proposed method, numerically simulated and tested in a physical quadcopter platform. Two different scenarios were used for the simulation results, which allowed us to verify the stability of the selected method for the three distinct controllers. All of them result in a stable response of the quadcopter platform while following the input trajectory. The experimental results were obtained in three different scenarios designed to test the robustness and agility of the three controllers. The resulting systems were stable even in the presence of perturbations or aggressive references. The fact that the simulation and experimental results did not diverge too far from one another speaks in favor of the exactitude and practical application of the presented method.

In general, it is preferable to design a controller for a completely actuated system than for an under actuated one. This is because the later includes dynamical dependencies between

state variables that can complicate the corroboration and design of control laws, which is not the case for fully actuated systems. The key advantage of the proposed design approach is that it can adapt a control strategy designed for fully actuated systems to be used in an under actuated platform. The sate-feedback controller shows that the algorithm can be used with linear controllers if one includes a gravity compensation term. The energy-shaping controller and the separated saturations control are examples of nonlinear control strategies that can also be adapted and used to the presented method.

Another popular approach to design controllers for the proposed family of under actuated systems is to use an internal attitude control loop to guide the actuator's force with an outer control loop. The stability results in these types of design strategies greatly depend on the robustness of the inner control loop. Even though the proposed strategy uses a similar approach, a key advantage of our method is that the stability of the whole system is guaranteed using the Lyapunov theory formalism. This makes the stability results be almost global and only limited by the physical properties of the platform itself. It can even lead to control strategies that work well for aggressive or rapid maneuvers of the platform, as the stability of the system can be analyzed as a whole instead of by parts.

References

Ahmad, F., Kumar, P., Bhandari, A., & Patil, P. P. (2020). Simulation of the quadcopter dynamics with lqr based control. *Materials Today: Proceedings*, *24*, 326-332. Retrieved from https://www.sciencedirect.com/science/article/pii/S2214785320329047 (International Conference on Advances in Materials and Manufacturing Applications, IConAMMA 2018, 16th -18th August, 2018, India)

Alatorre, A. G., Castillo, P., & Mondié, S. (2016). Saturations-based nonlinear controllers with integral term: validation in real-time. *International Journal of Control*, *89*(5), 879–891.

Altmann, S. L. (1989). Hamilton, rodrigues, and the quaternion scandal. *Mathematics Magazine*, *62*(5), 291–308.

Antonio-Toledo, M. E., Sanchez, E. N., Alanis, A. Y., Flórez, J., & Perez-Cisneros, M. A. (2018). Real-time integral backstepping with sliding mode control for a quadrotor uav. *IFAC-PapersOnLine*, *51*(13), 549-554. Retrieved from https://www.sciencedirect.com/science/article/pii/S2405896318310929 (2nd IFAC Conference on Modelling, Identification and Control of Nonlinear Systems MICNON 2018)

Ariyibi, S. O., & Tekinalp, O. (2020). Quaternion-based nonlinear attitude control of quadrotor formations carrying a slung load. *Aerospace Science and Technology*, *105*, 105995. Retrieved from https://www.sciencedirect.com/science/article/pii/S1270963820306775

Brogliato, B., Maschke, B., Lozano, R., & Egeland, O. (2007). Passivity-based control. In *Dissipative systems analysis and control: Theory and applications* (pp. 373–434). London: Springer London.

Campa, R., & Camarillo, K. (2008). Unit quaternions: A mathematical tool for modeling, path planning and control of robot manipulators. In M. Ceccarelli (Ed.), *Robot manipulators* (p. 21-48). Rijeka: IntechOpen. Retrieved from https://doi.org/10.5772/6197

Castillo, P., Dzul, A., & Lozano, R. (2004). Real-time stabilization and tracking of a four-rotor mini rotorcraft. *IEEE Transactions on Control Systems Technology*, *12*(4), 510-516.

Colmenares-Vázquez, J., Marchand, N., Castillo, P., & Gómez-Balderas, J. E. (2017). An intermediary quaternion-based control for trajectory following using a quadrotor. In *2017 ieee/rsj international conference on intelligent robots and systems (iros)* (p. 5965-5970).

El-Badawy, A. A., & Bakr, M. A. (2016, Jan 18). Quadcopter aggressive maneuvers along singular configurations: An energy-quaternion based approach. *Journal of Control Science and Engineering*, *2016*, 7324540. Retrieved from https://doi.org/10.1155/2016/7324540

Fritsch, O., Tromba, D., & Lohmann, B. (2014, Jun). Cascaded energy based trajectory tracking control of a quadrotor. *Automatisierungstechnik*, *62*(6), 408–422.

Goldstein, H., Poole, C., & Safko, J. (2002). *Classical mechanics*. Addison Wesley. Retrieved from https://books.google.com.mx/books?id=EE-wQgAACAAJ

Hancock, P. A., Nourbakhsh, I., & Stewart, J. (2019). On the future of transportation in an era of automated and autonomous vehicles. *Proceedings of the National Academy of Sciences*, *116*(16),

7684–7691. Retrieved from https://www.pnas.org/content/116/16/7684
Islam, M., & Okasha, M. (2019). A comparative study of pd, lqr and mpc on quadrotor using quaternion approach. In *2019 7th international conference on mechatronics engineering (icom)* (p. 1-6).
Islam, M., Okasha, M., Idres, M., & Mansor, H. (2018, 10). Trajectory tracking of quaternion based quadrotor using model predictive control. *International Journal of Engineering and Technology(UAE)*, *7*, 125-136.
Kalman, D. (1989). The axis of a rotation: Analysis, algebra, geometry. *Mathematics Magazine*, *62*(4), 248-252. Retrieved from https://doi.org/10.1080/0025570X.1989.11977446
Kopelias, P., Demiridi, E., Vogiatzis, K., Skabardonis, A., & Zafiropoulou, V. (2020). Connected & autonomous vehicles – environmental impacts – a review. *Science of The Total Environment*, *712*, 135237.
Kottenstette, N., & Porter, J. (2009). Digital passive attitude and altitude control schemes for quadrotor aircraft. In *2009 ieee international conference on control and automation* (p. 1761-1768).
Kuipers, J. B., et al. (1999). *Quaternions and rotation sequences* (Vol. 66). Princeton university press Princeton.
Kumar, R., Bhargavapuri, M., Deshpande, A. M., Sridhar, S., Cohen, K., & Kumar, M. (2020). Quaternion feedback based autonomous control of a quadcopter uav with thrust vectoring rotors. In *2020 american control conference (acc)* (p. 3828-3833).
Labbadi, M., & Cherkaoui, M. (2019). Robust adaptive backstepping fast terminal sliding mode controller for uncertain quadrotor uav. *Aerospace Science and Technology*, *93*, 105306. Retrieved from https://www.sciencedirect.com/science/article/pii/S1270963819300318
Lees-Miller, J. D., Hammersley, J. C., & Wilson, R. E. (2010). Theoretical maximum capacity as benchmark for empty vehicle redistribution in personal rapid transit. *Transportation Research Record*, *2146*(1), 76-83. Retrieved from https://doi.org/10.3141/2146-10
Li, S., Sui, P.-C., Xiao, J., & Chahine, R. (2019). Policy formulation for highly automated vehicles: Emerging importance, research frontiers and insights. *Transportation Research Part A: Policy and Practice*, *124*, 573-586. Retrieved from https://www.sciencedirect.com/science/article/pii/S0965856418300430
Lu, Q., Ren, B., & Parameswaran, S. (2020). Uncertainty and disturbance estimator-based global trajectory tracking control for a quadrotor. *IEEE/ASME Transactions on Mechatronics*, *25*(3), 1519-1530.
Markley, F. L. (2002). Fast quaternion attitude estimation from two vector measurements. *Journal of Guidance, Control, and Dynamics*, *25*(2), 411-414. Retrieved from https://doi.org/10.2514/2.4897
Morais, J. P., Georgiev, S., & Sprößig, W. (2014a). Exponents and logarithms. In *Real quaternionic calculus handbook* (pp. 87–105). Basel: Springer Basel.
Morais, J. P., Georgiev, S., & Sprößig, W. (2014b). Quaternions and spatial rotation. In *Real quaternionic calculus handbook* (pp. 35–51). Basel: Springer Basel.
Muñoz, L. E., Santos, O., Castillo, P., & Fantoni, I. (2013). Energy-based nonlinear control for a quadrotor rotorcraft. In *2013 american control conference* (p. 1177-1182).
Pratama, B., Muis, A., Subiantoro, A., Djemai, M., & Ben Atitallah, R. (2018, October 1). Quadcopter trajectory tracking and attitude control based on euler angle limitation. In D. Arisoy, S. Engin, & M. Oz (Eds.), *2018 6th international conference on control engineering and information technology, ceit 2018*. United States: Institute of Electrical and Electronics Engineers Inc. (6th International Conference on Control Engineering and Information Technology, CEIT 2018 ; Conference date: 25-10-2018 Through 27-10-2018)
Sanahuja, G. (2016). *Fl-air - framework libre air.* Retrieved from https://devel.hds.utc.fr/software/flair ([Online; accessed 19-April-2021])
Shastry, A. K., Bhargavapuri, M. T., Kothari, M., & Sahoo, S. R. (2018). Quaternion based adaptive control for package delivery using variable-pitch quadrotors. In *2018 indian control conference (icc)* (p. 340-345).
Shuster, M. D. (1993, October). Survey of attitude representations. *Journal of the Astronautical Sciences*, *41*(4), 439-517.
Souza, C., Raffo, G., & Castelan, E. (2014). Passivity based control of a quadrotor uav. *IFAC Proceedings Volumes*, *47*(3), 3196-3201. Retrieved from https://www.sciencedirect.com/science/article/pii/S1474667016420999 (19th IFAC World Congress)
Xie, H., & Lynch, A. F. (2017). Input saturated visual servoing for unmanned aerial vehicles.

IEEE/ASME Transactions on Mechatronics, *22*(2), 952-960.

Appendix A. Quaternion Background

Quaternions, also called hyper-complex numbers and represented with an $\mathbb{H}$, are a special group that form an algebraic ring with division. They were first described by Irish mathematician Sir William Rowan Hamilton Altmann (1989) .

They can be represented in many ways, but the one presented here is as a sum of a scalar component along an imaginary vector as seen in Campa and Camarillo (2008) and Kuipers et al. (1999).

$$\boldsymbol{q} = q_0 + \vec{q} = q_0 + \begin{bmatrix} q_1 & q_2 & q_3 \end{bmatrix}^T \tag{A1}$$

where $\boldsymbol{q} \in \mathbb{H}$, $\bar{q} \in \mathbb{R}^3$ depicts the complex vectorial part of $\boldsymbol{q}$, and $q_0 \in \mathbb{R}$ denotes the scalar part of $\boldsymbol{q}$.

A.1. Quaternion Product

The main operation in quaternion algebra is the quaternion product, which is defined as

$$\boldsymbol{q} \otimes \boldsymbol{r} = (q_0\, r_0 - \vec{q} \cdot \vec{r}) + (r_0\, \vec{q} + q_0\, \vec{r} + \vec{q} \times \vec{r}) \tag{A2}$$

where $\boldsymbol{r} \in \mathbb{H}$, with vector part $\vec{r} \in \mathbb{R}^3$ and scalar part $r_0 \in \mathbb{R}$.

A.2. Quaternion Conjugate and Norm

The quaternion conjugate $\boldsymbol{q}^* \in \mathbb{H}$ is defined as $\boldsymbol{q}^* = q_0 - \vec{q}$, while the quaternion norm, $\|\boldsymbol{q}\| \in \mathbb{R}$, is defined as

$$\|\boldsymbol{q}\| = \sqrt{\boldsymbol{q} \otimes \boldsymbol{q}^*} = \sqrt{q_0^2 + q_1^2 + q_2^2 + q_3^2} \tag{A3}$$

A.3. Quaternion Inverse

The quaternion inverse is obtained from $\boldsymbol{q}^{-1} = \dfrac{\boldsymbol{q}^*}{\|\boldsymbol{q}\|}$. Only unit quaternions are used for the attitude representation of a rigid body, that is $\|\boldsymbol{q}\| = 1$. Thus, $\boldsymbol{q}^{-1} = \boldsymbol{q}^*$.

A.4. Quaternion Scalar and Vector Parts

Even though it was mentioned at the beginning of the section that any quaternion can be expressed as the sum of a real scalar component and a vector imaginary part, there are still operations and analysis that would benefit from an operation design to extract either of these components. In order to achieve this, two operations are defined for an arbitrary quaternion $\boldsymbol{q} \in \mathbb{H}$. The first one extracts the real scalar part

$$Sca\,\{\boldsymbol{q}\} \coloneqq \frac{1}{2}\,(\boldsymbol{q} - \boldsymbol{q}^*) = q_0 \tag{A4}$$

while the second one extracts the imaginary vector part

$$Vec\{\boldsymbol{q}\} \coloneqq \frac{1}{2}(\boldsymbol{q} + \boldsymbol{q}^*) = \vec{q} \tag{A5}$$

A.5. Quaternion Natural Logarithm

The quaternion natural logarithm mapping is defined as R1Q3

$$\ln \boldsymbol{q} = \begin{cases} \ln \|\boldsymbol{q}\| + \dfrac{\vec{q}}{\|\vec{q}\|} arccos\ \dfrac{q_0}{\|\boldsymbol{q}\|}, & \|\vec{q}\| \neq 0 \\ \ln \|\boldsymbol{q}\|, & \|\vec{q}\| = 0 \end{cases} \tag{A6}$$

For unit quaternions, the above logarithmic mapping is reduced to R1Q3

$$\ln \boldsymbol{q} = \begin{cases} \dfrac{\vec{q}}{\|\vec{q}\|} arccos\ q_0, & \|\vec{q}\| \neq 0 \\ 0, & \|\vec{q}\| = 0 \end{cases} \tag{A7}$$

This mapping is useful to change any unit quaternion to the axis-angle representation, in which the quaternion is represented as an axis over which the vehicle will rotate, and a rotation angle.

$$\frac{\vec{\theta}}{2} = \ln \boldsymbol{q}, \quad \dot{\vec{\theta}} = \omega \tag{A8}$$

where $\bar{\theta} \in \mathbb{R}^3$ is the vector which contains the axis-angle representation, in which $\frac{\bar{\theta}}{\|\bar{\theta}\|}$ describes the unitary axis over which the rotation is applied, $\|\bar{\theta}\|$ represents the magnitude of the rotation, and ω is the vehicle's angular velocity.

A.6. Quaternion kinematics

The kinematics of a rigid body in terms of its orientation and the angular velocity with respect to the body frame are given in Goldstein et al. (2002) by

$$\dot{\boldsymbol{q}} = \frac{1}{2}\boldsymbol{q} \otimes \omega \tag{A9}$$